Note after first publication: *This document replaces the version originally published on 1st March, which had errors in Table S4.*

Supporting Information

Investigating the anticancer potential of 4-phenylthiazole derived Ru(II) and Os(II) metalacycles

Paul Getreuer, [a,b] Laura Marretta,[c] Emine Toyoglu,[a] Orsolya Dömötör,[d] Michaela Hejl,[a] Alexander Prado-Roller,[a] Klaudia Cseh,[a] Anton A. Legin,[a] Michael A. Jakupec,[a,e] Giampaolo Barone,[c] Alessio Terenzi,[c] Bernhard Keppler, [a,e] and Wolfgang Kandioller [a,e,*]

[a]Institute of Inorganic Chemistry, Faculty of Chemistry, University of Vienna, Waehringer Straße 42, 1090 Vienna, Austria.

[b]Vienna Doctoral School in Chemistry (DoSChem), Faculty of Chemistry, University of Vienna, Waehringer Straße 42, 1090 Vienna, Austria.

[c]STEBICEF-Department, University of Palermo, Viale delle Scienze, Ed. 17, 90128 Palermo, Italy.

[d]Department of Molecular and Analytical Chemistry, University of Szeged, Dóm tér 7-8, 6720 Szeged, Hungary.

[e]Research Cluster "Translational Cancer Therapy Research", University of Vienna, Waehringer Straße 42, 1090 Vienna, Austria.

1. Synthesis of 4-phenylthiazole ligands (1a-e)

General procedure. The general procedure was adapted from Lee *et al*.[1] 4-Bromothiazole (1.0 eq.), the respective boronic acid or boronic ester (1.5 eq.) and K_2CO_3 (2.0 eq.) were suspended in a 3:1 dioxane/H_2O mixture (8 mL) and degassed with Ar. Subsequently, tetrakis(triphenylphosphine)Pd(0) (0.02 eq.) was added and the mixture was heated to 100 °C in a sealed vial. After TLC showed full conversion the mixture was partitioned between H_2O and EtOAc and the aqueous layer was further extracted with EtOAc (2x). The combined organic extracts were washed with brine, dried over Na_2SO_4, filtered and concentrated under reduced pressure. After purification *via* column chromatography and drying for 2 days at room temperature *in vacuo*, the respective 4-phenylthiazole was obtained in elemental analysis purity.

4-Phenylthiazole (1a). The reaction was performed according to the general procedure, using 4-bromothiazole (984 mg, 6 mmol), 4,4,5,5-tetramethyl-2-phenyl-1,3,2-dioxaborolane (1.837 g, 9 mmol), K_2CO_3 (1.658 g, 12 mmol) and tetrakis(triphenylphosphine)Pd(0) (139 mg, 120 µmol) with a reaction time of 21 h (5% EtOAc in *n*-hexane, 867 mg, 89% yield). Elemental analysis found (calculated) for C_9H_7NS: C 66.71 (67.05), H 4.25 (4.38), N 8.65 (8.69), S 20.10 (19.89), O <0.05 (0.00). ^{1}H NMR (500.10 MHz, $CDCl_3$): δ = 8.89 (d, $^4J_{H,H}$ = 2 Hz, 1H, $ArH_{Th\text{-}2}$), 7.94 (ddd, $^3J_{H,H}$ = 8.2, $^4J_{H,H}$ = 1.6 Hz, 2H, $ArH_{Ph\text{-}2,\ Ph\text{-}6}$), 7.55 (d, $^4J_{H,H}$ = 2.0 Hz, 1H, $ArH_{Th\text{-}5}$), 7.47–7.42 (m, 2H, $ArH_{Ph\text{-}3,\ Ph\text{-}5}$), 7.39–7.33 (m, 1H, $ArH_{Ph\text{-}4}$) ppm.

4-(4-Fluorophenyl)thiazole (1b). The reaction was performed according to the general procedure, using 4-bromothiazole (984 mg, 6 mmol), (4-fluorophenyl)boronic acid (1.260 g, 9 mmol), K_2CO_3 (1.658 g, 12 mmol) and tetrakis(triphenylphosphine)Pd(0) (139 mg, 120 µmol) with a reaction time of 23 h (5% EtOAc in *n*-hexane, 454 mg, 42% yield). Elemental analysis found (calculated) for C_9H_6FNS: C 60.24 (60.32), H 3.41 (3.37), N 7.57 (7.82), S 17.84 (17.89), O 0.21 (0.00). ^{1}H NMR (500.10 MHz, $CDCl_3$): δ = 8.87 (d, $^4J_{H,H}$ = 2 Hz, 1H, $ArH_{Th\text{-}2}$), 7.98–7.85 (m, 2H, $ArH_{Ph\text{-}2,\ Ph\text{-}6}$), 7.48 (d, $^4J_{H,H}$ = 2 Hz, 1H, $ArH_{Th\text{-}5}$), 7.18–7.07 (m, 2H, $ArH_{Ph\text{-}3,\ Ph\text{-}5}$) ppm.

4-(4-(Methylsulfonyl)phenyl)thiazole (1c). The reaction was performed according to the general procedure, using 4-bromothiazole (984 mg, 6 mmol), (4-(methylsulfonyl)phenyl)boronic acid (1.800 g, 9 mmol), K_2CO_3 (1.658 g, 12 mmol) and tetrakis(triphenylphosphine)Pd(0) (139 mg, 120 µmol) with a reaction time of 23 h (40-50% EtOAc in *n*-hexane, 925 mg, 64% yield). Elemental analysis found (calculated) for $C_{10}H_9NO_2S_2 \cdot 0.10\ H_2O$: C 49.78 (49.81), H 3.72 (3.85), N 5.62 (5.81), S 26.66 (26.60), O 13.59 (13.93). ^{1}H NMR (500.10 MHz, $CDCl_3$): δ = 8.93 (d, $^4J_{H,H}$ = 2 Hz, 1H, $ArH_{Th\text{-}2}$), 8.16–8.13 (m, 2H, $ArH_{Ph\text{-}2,\ Ph\text{-}6}$), 8.04–7.98 (m, 2H, $ArH_{Ph\text{-}3,\ Ph\text{-}5}$), 7.74 (d, $^4J_{H,H}$ = 2 Hz, 1H, $ArH_{Th\text{-}5}$), 3.09 (s, 3H, CH_3) ppm.

4-(4-Methylphenyl)thiazole (1d). The reaction was performed according to the general procedure, using 4-bromothiazole (984 mg, 6 mmol), 4,4,5,5-tetramethyl-2-(4-methylphenyl)-1,3,2-dioxaborolane (1.963 g, 9 mmol), K_2CO_3 (1.658 g, 12 mmol) and tetrakis(triphenylphosphine)Pd(0) (139 mg, 120 µmol) with a reaction time of 23 h (5% EtOAc in *n*-hexane, 902 mg, 86% yield). Elemental analysis found (calculated) for $C_{10}H_9NS$: C 68.18 (68.54), H 5.09 (5.18), N 7.89 (7.99), S 18.48 (18.29), O <0.05 (0.00). ^{1}H NMR (500.10 MHz, $CDCl_3$): δ = 8.87 (d, $^4J_{H,H}$ = 2 Hz, 1H, $ArH_{Th\text{-}2}$), 7.83 (d, $^3J_{H,H}$ = 8 Hz, 2H, $ArH_{Ph\text{-}2,\ Ph\text{-}6}$), 7.48 (d, $^4J_{H,H}$ = 2 Hz, 1H, $ArH_{Th\text{-}5}$), 7.26–7.24 (m, 2H, $ArH_{Ph\text{-}3,\ Ph\text{-}5}$), 2.39 (s, 3H, CH_3) ppm.

4-(4-Methoxyphenyl)thiazole (1e). The reaction was performed according to the general procedure, using 4-bromothiazole (984 mg, 6 mmol), 2-(4-methoxyphenyl)-4,4,5,5-tetramethyl-1,3,2-dioxaborolane (2.107 g, 9 mmol), K_2CO_3 (1.658 g, 12 mmol) and tetrakis(triphenylphosphine)Pd(0) (139 mg, 120 µmol) with a reaction time of 23 h (10% EtOAc in *n*-hexane, 998 mg, 87% yield). Elemental analysis found (calculated) for $C_{10}H_9NOS$: C 62.57 (62.80), H 4.67 (4.74), N 7.28 (7.32), S 16.85 (16.76), O 8.42 (8.37). ^{1}H NMR (500.10 MHz, $CDCl_3$): δ = 8.86 (d, $^4J_{H,H}$ = 2 Hz, 1H, $ArH_{Th\text{-}2}$), 7.91–7.84 (m, 2H, $ArH_{Ph\text{-}2,\ Ph\text{-}6}$), 7.40 (d, $^4J_{H,H}$ = 2.0 Hz, 1H, $ArH_{Th\text{-}5}$), 7.00–6.94 (m, 2H, $ArH_{Ph\text{-}3,\ Ph\text{-}5}$), 3.86 (s, 3H, CH_3) ppm.

2. ^{1}H and ^{13}C NMR Spectra

4-Phenylthiazole (1a)

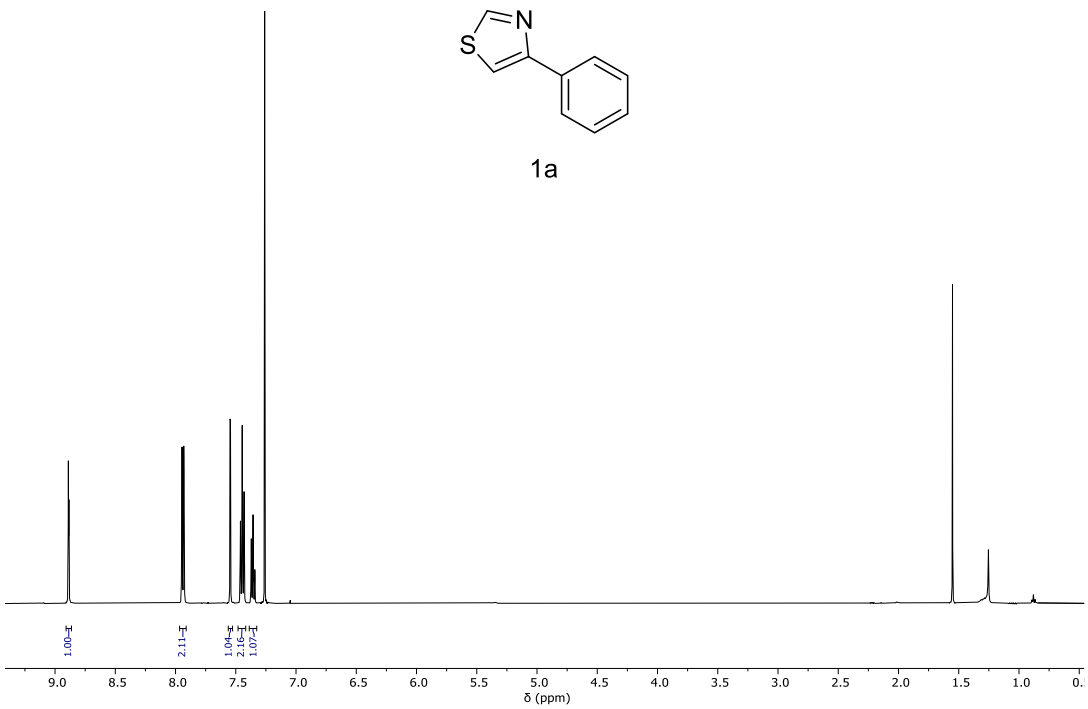

Figure S1: ^{1}H NMR of **1a** in $CDCl_3$.

4-(4-Fluorophenyl)thiazole (1b)

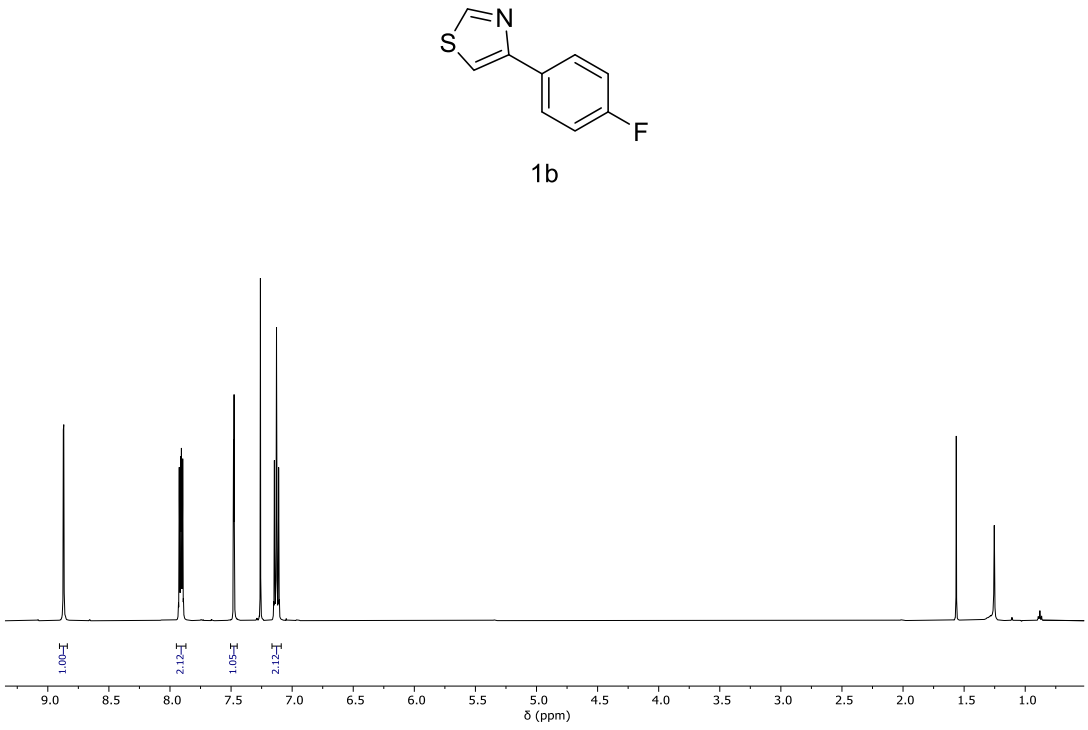

Figure S2: ^{1}H NMR of **1b** in $CDCl_3$.

4-(4-(Methylsulfonyl)phenyl)thiazole (1c)

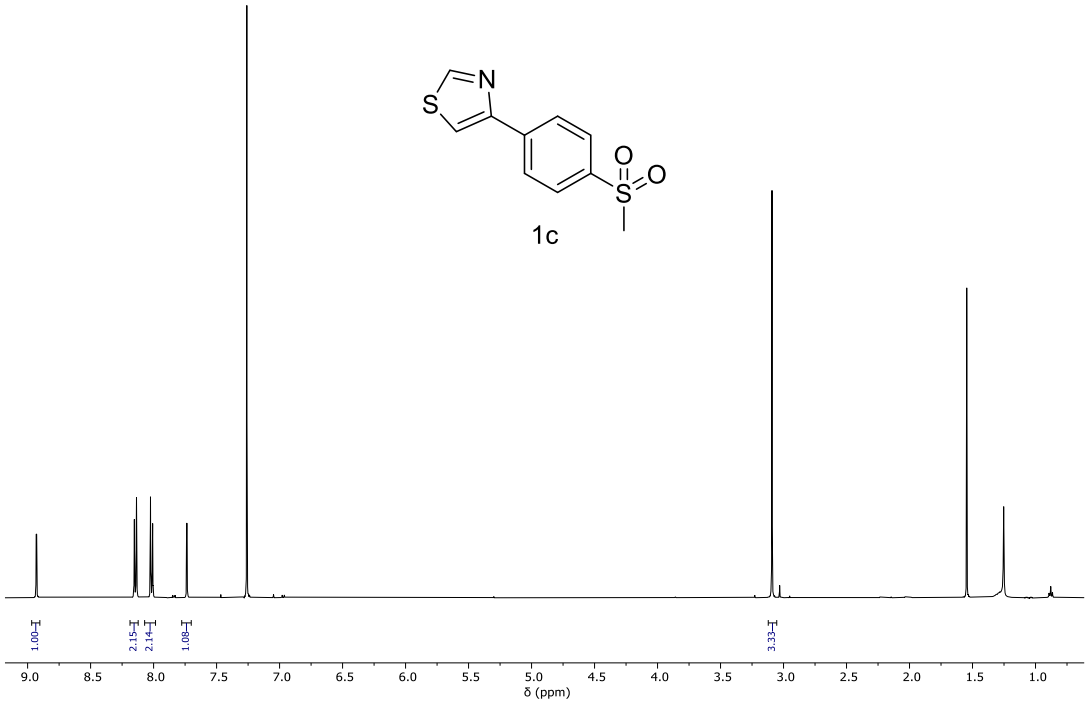

Figure S3: ^{1}H NMR of **1c** in $CDCl_3$.

4-(4-Methylphenyl)thiazole (1d)

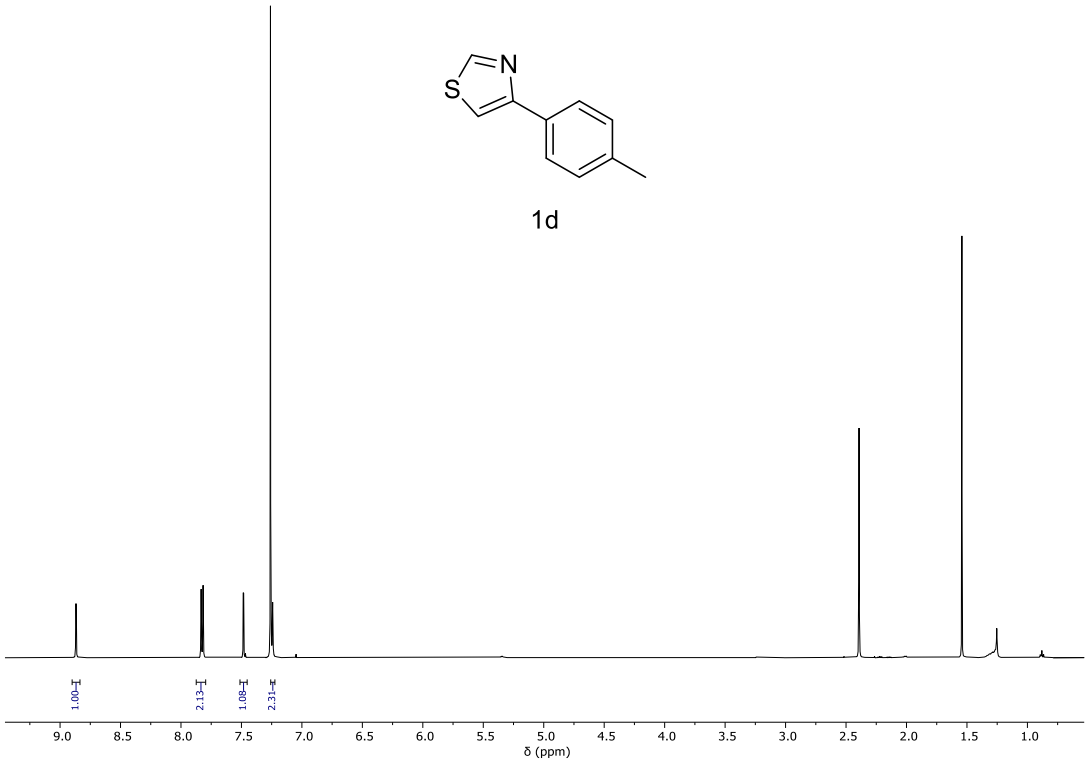

Figure S4: ^{1}H NMR of **1d** in $CDCl_3$.

4-(4-Methoxyphenyl)thiazole (1e)

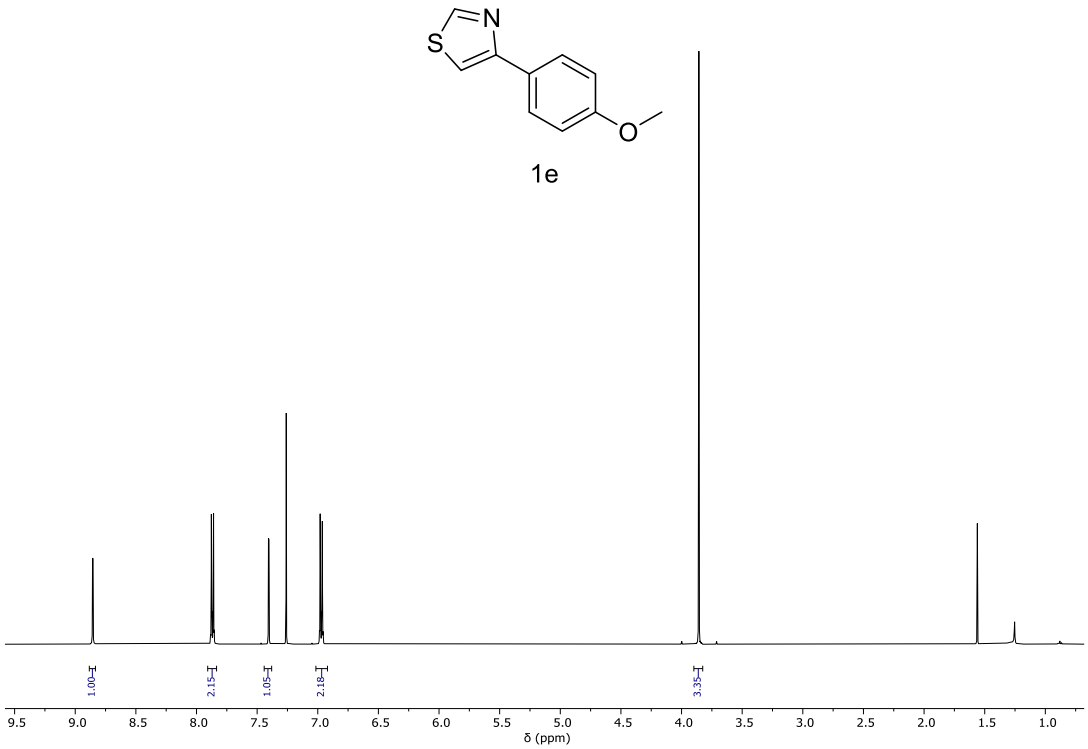

Figure S5: ^{1}H NMR of **1e** in $CDCl_3$.

[(Chlorido)(4-phenylthiazolato-κN,κC2´)(η^6-*p*-cymene)ruthenium(II)] (2a)

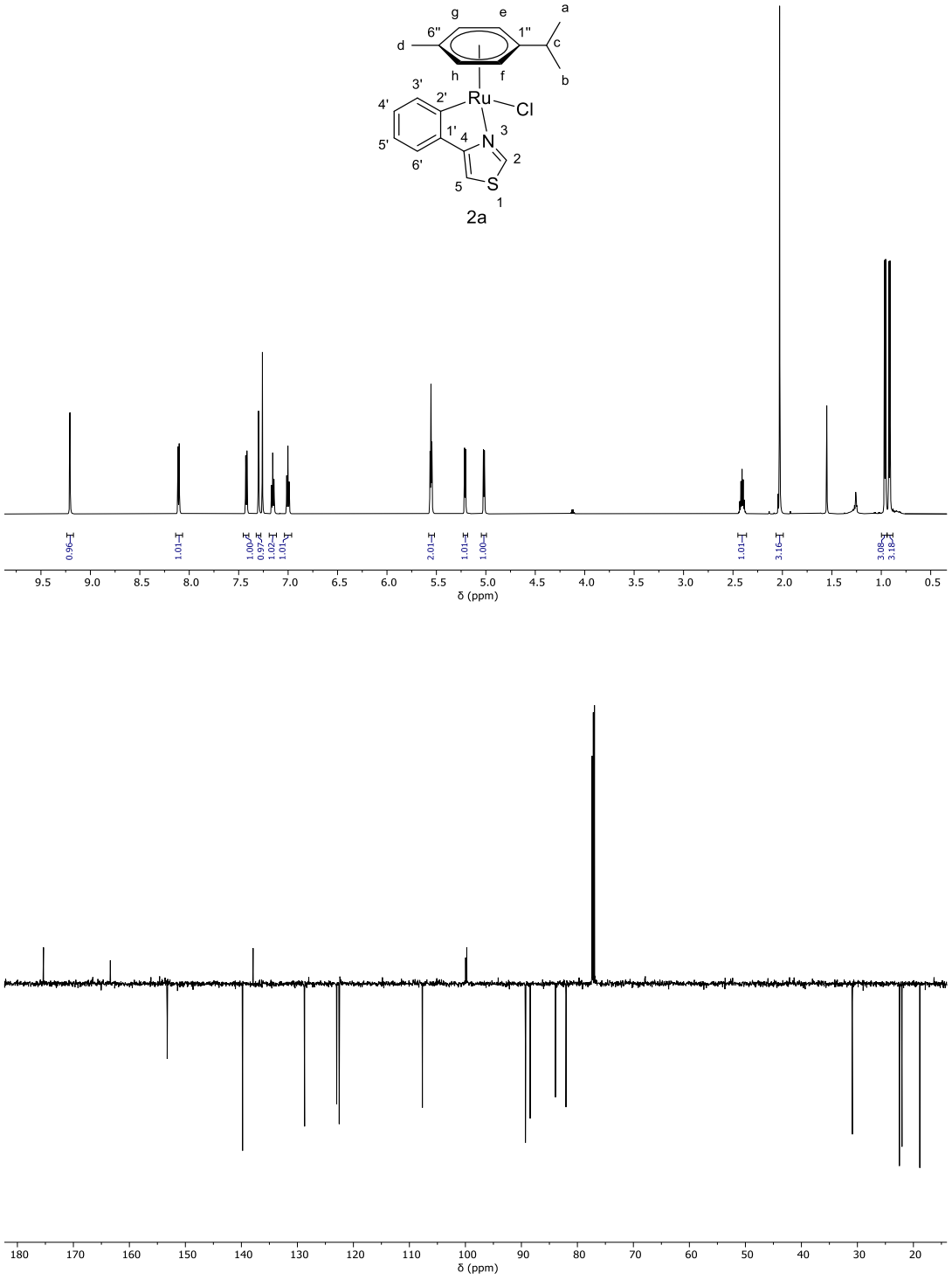

Figure S6: Atom numbering (above), ^{1}H (center) and ^{13}C (below) NMR of **2a** in $CDCl_3$.

[(Chlorido)(4-(4-fluorophenyl)thiazolato-κN,κC2´)(η^6-*p*-cymene)ruthenium(II)] (2b)

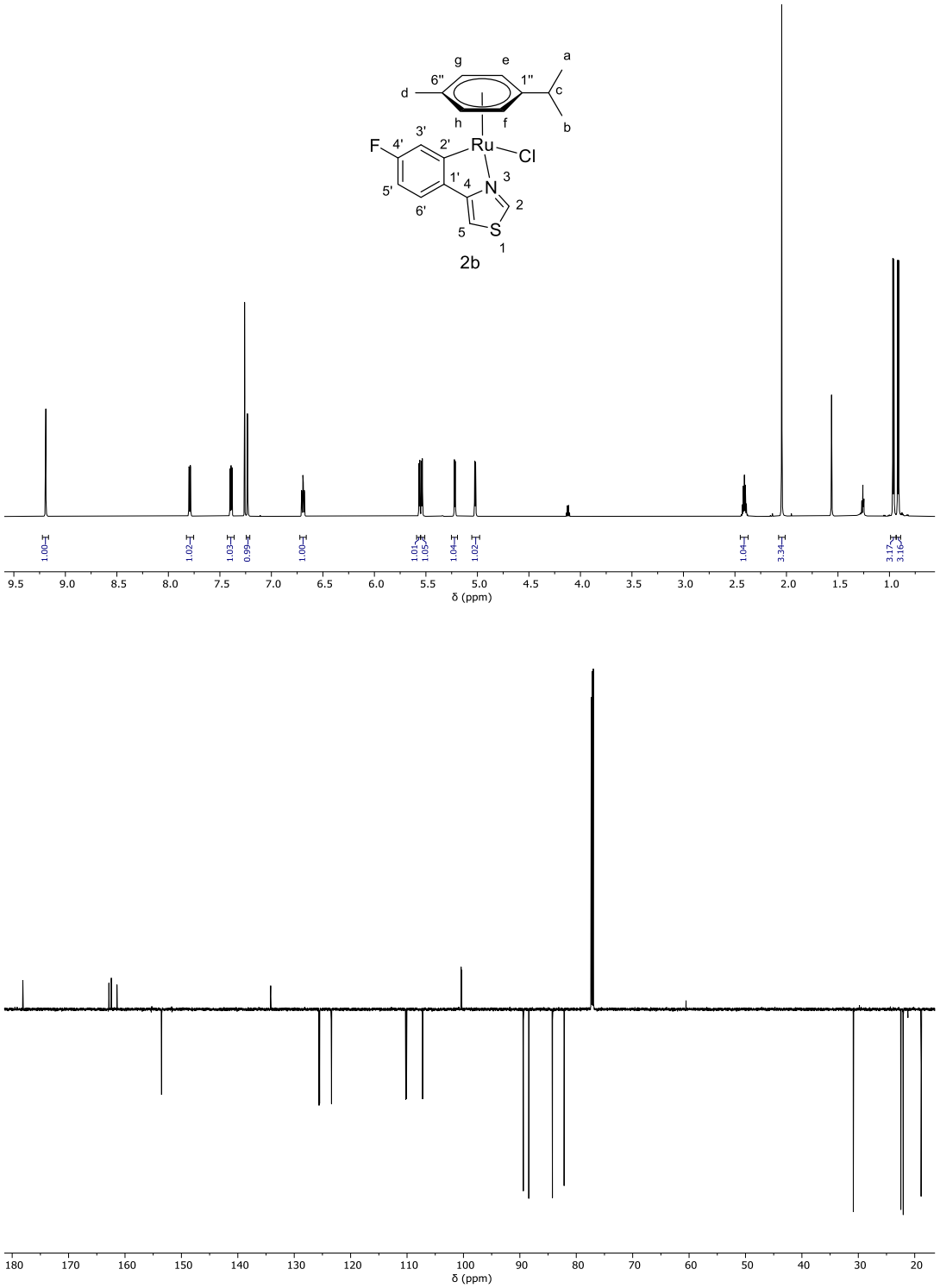

Figure S7: Atom numbering (above), ^{1}H (center) and ^{13}C (below) NMR of **2b** in $CDCl_3$.

[(Chlorido)(4-(4-(methylsulfonyl)phenyl)thiazolato-κN,κC2´)(η^6-*p*-cymene)ruthenium(II)] (2c)

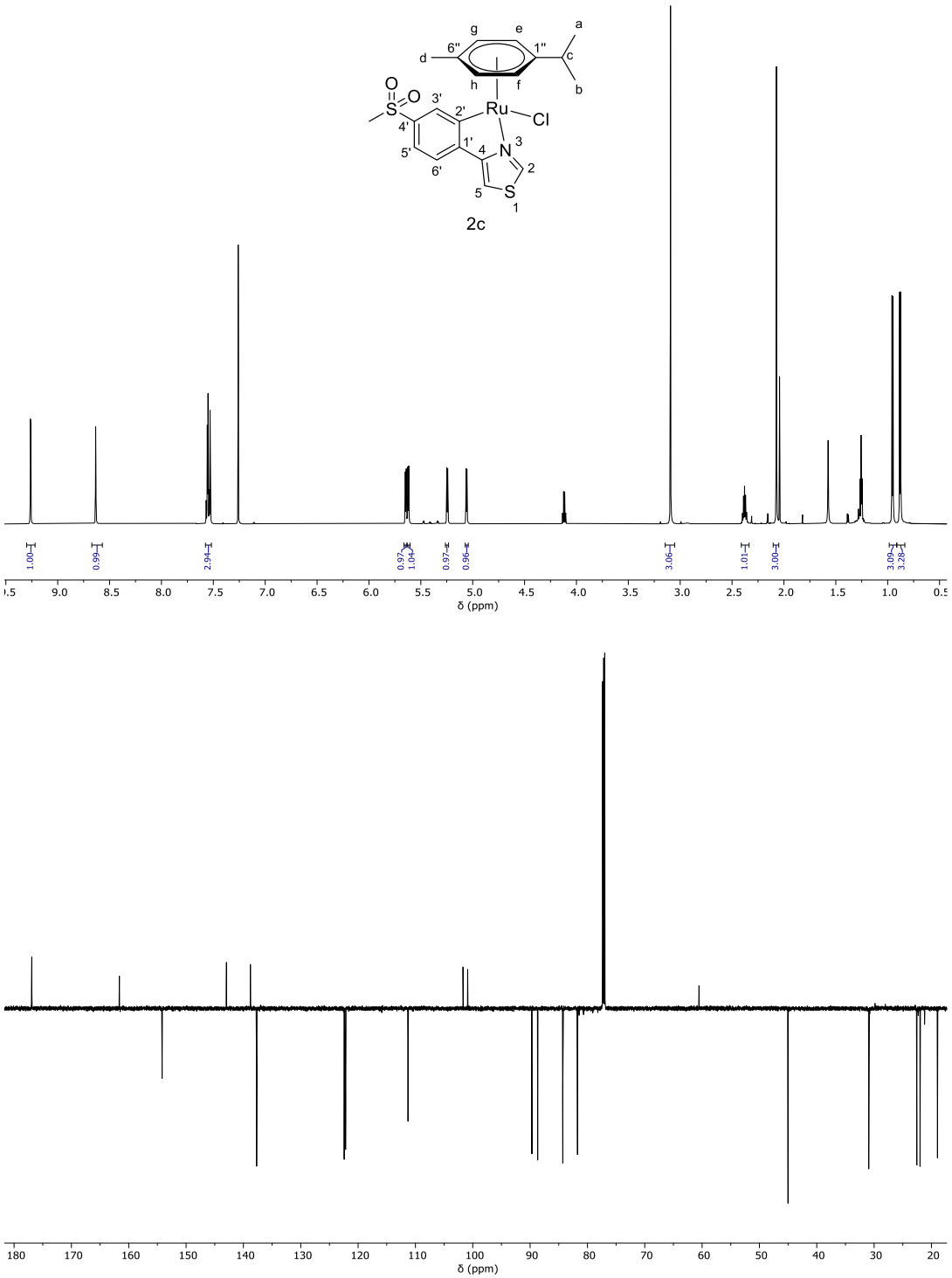

Figure S8: Atom numbering (above), ^{1}H (center) and ^{13}C (below) NMR of **2c** in $CDCl_3$.

[(Chlorido)(4-(4-methylphenyl)thiazolato-κN,κC2´)(η^6-*p*-cymene)ruthenium(II)] (2d)

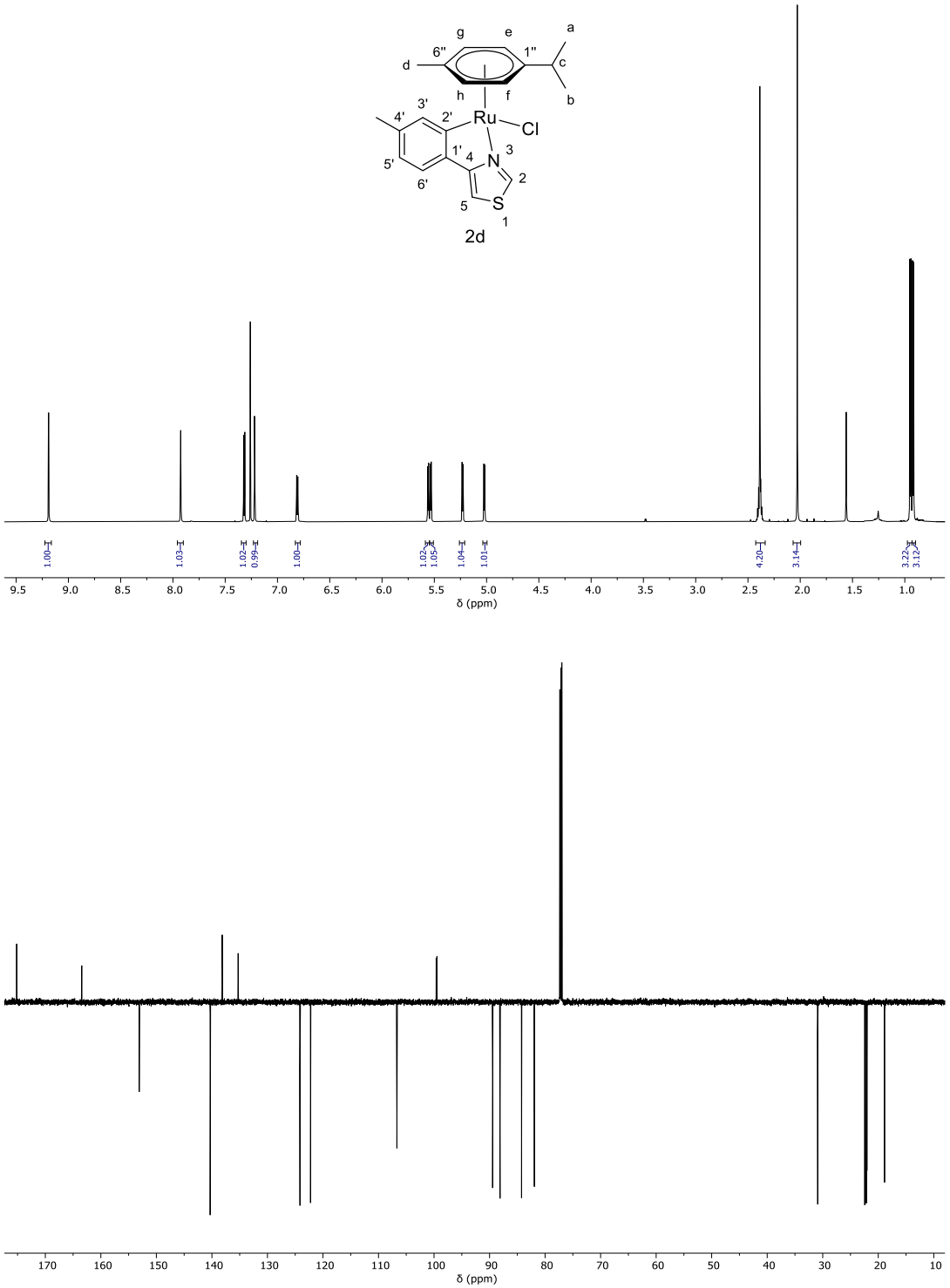

Figure S9: Atom numbering (above), ^{1}H (center) and ^{13}C (below) NMR of **2d** in $CDCl_3$.

[(Chlorido)(4-(4-methoxyphenyl)thiazolato-κN,κC2´)(η^6-*p*-cymene)ruthenium(II)] (2e)

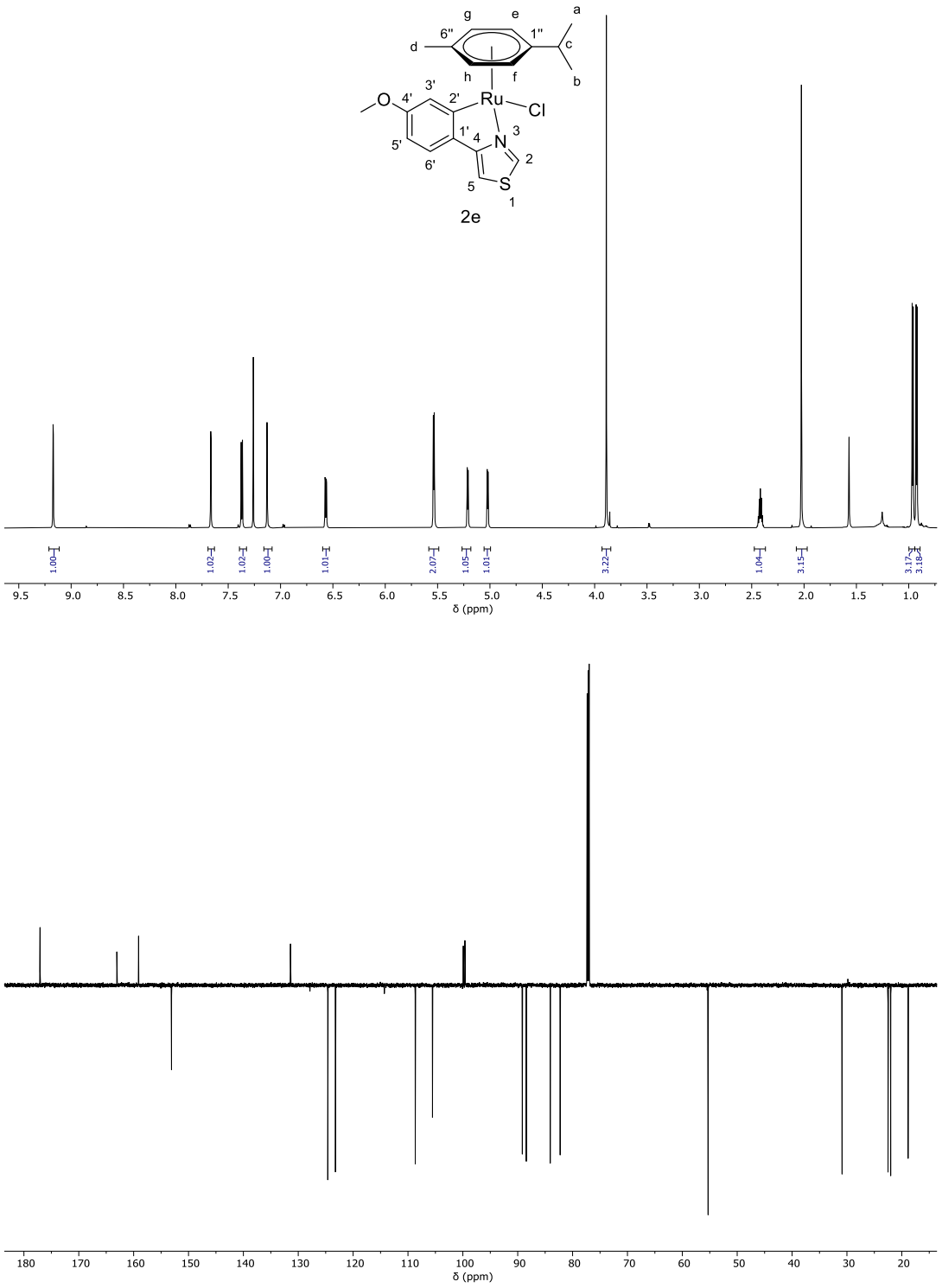

Figure S10: Atom numbering (above), ^{1}H (center) and ^{13}C (below) NMR of **2e** in $CDCl_3$.

[(Chlorido)(4-phenylthiazolato-κN,κC2´)(η^6-*p*-cymene)osmium(II)] (3a)

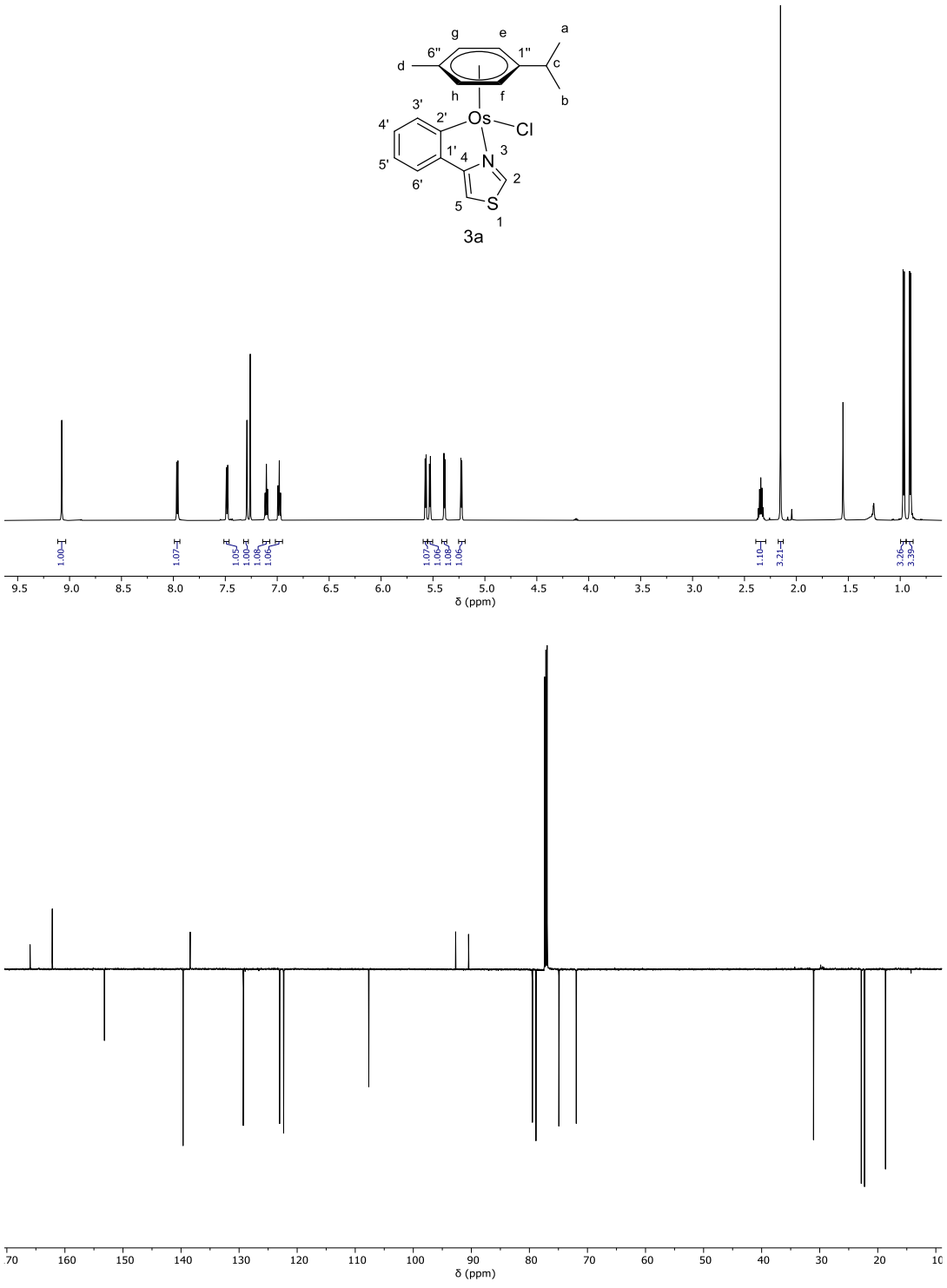

Figure S11: Atom numbering (above), ^{1}H (center) and ^{13}C (below) NMR of **3a** in $CDCl_3$.

[(Chlorido)(4-(4-fluorophenyl)thiazolato-κN,κC2´)(η^6-*p*-cymene)osmium(II)] (3b)

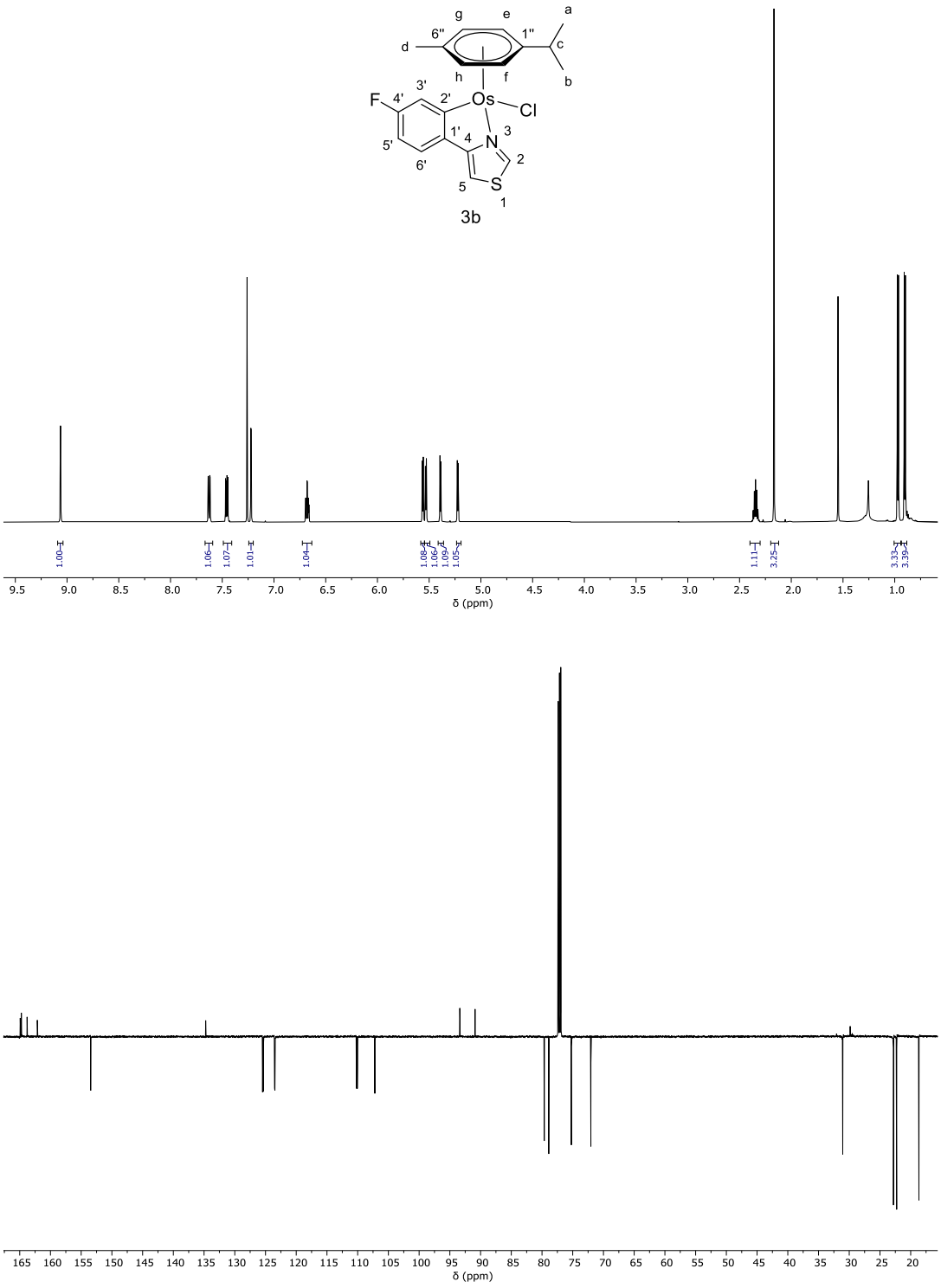

Figure S12: Atom numbering (above), ^{1}H (center) and ^{13}C (below) NMR of **3b** in $CDCl_3$.

[(Chlorido)(4-(4-(methylsulfonyl)phenyl)thiazolato-κN,κC2´)(η^6-*p*-cymene)osmium(II)] (3c)

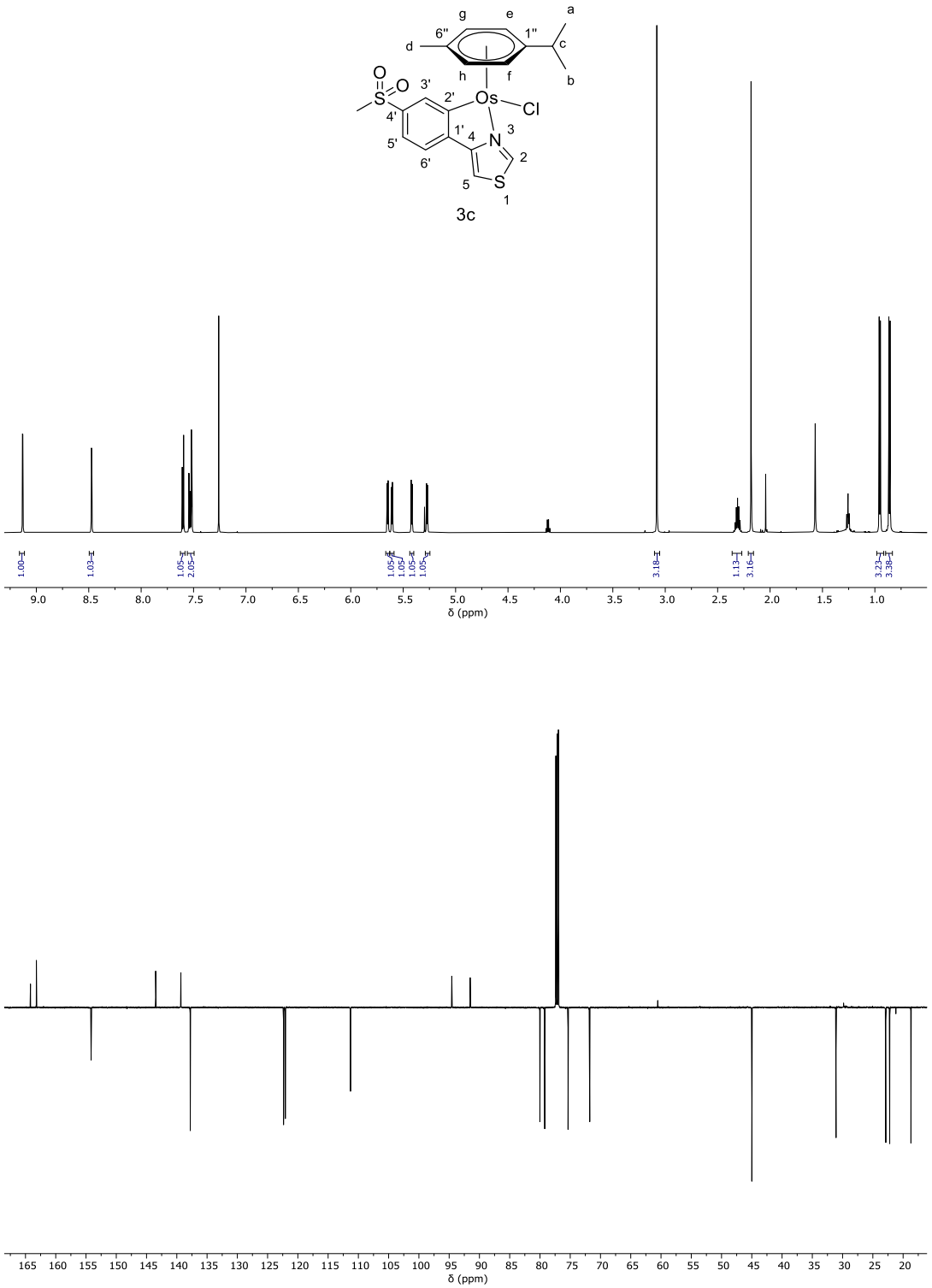

Figure S13: Atom numbering (above), ^{1}H (center) and ^{13}C (below) NMR of **3c** in $CDCl_3$.

[(Chlorido)(4-(4-methylphenyl)thiazolato-κN,κC2´)(η^6-*p*-cymene)osmium(II)] (3d)

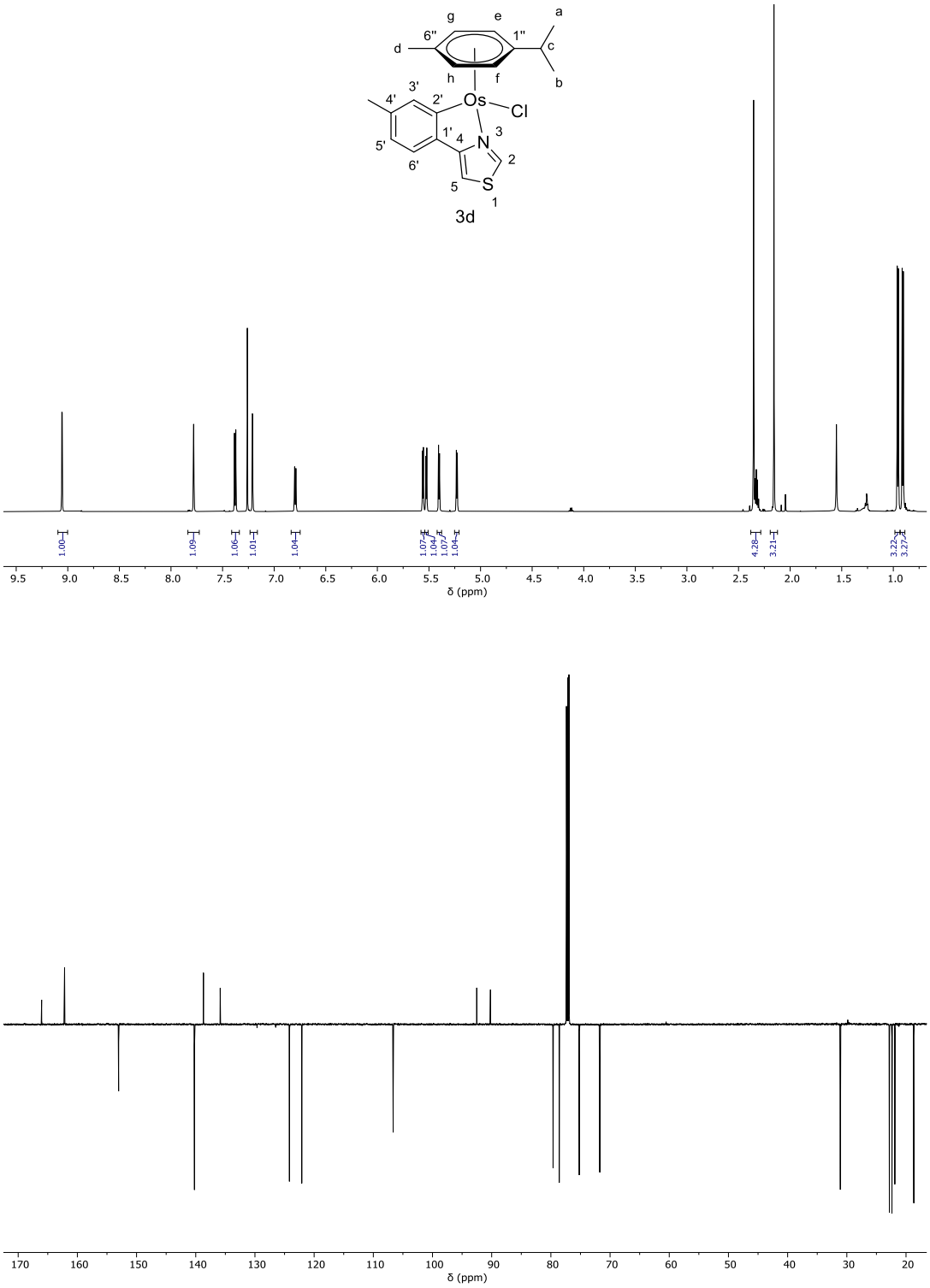

Figure S14: Atom numbering (above), ^{1}H (center) and ^{13}C (below) NMR of **3d** in $CDCl_3$.

[(Chlorido)(4-(4-methoxyphenyl)thiazolato-κN,κC2´)(η^6-*p*-cymene)osmium(II)] (3e)

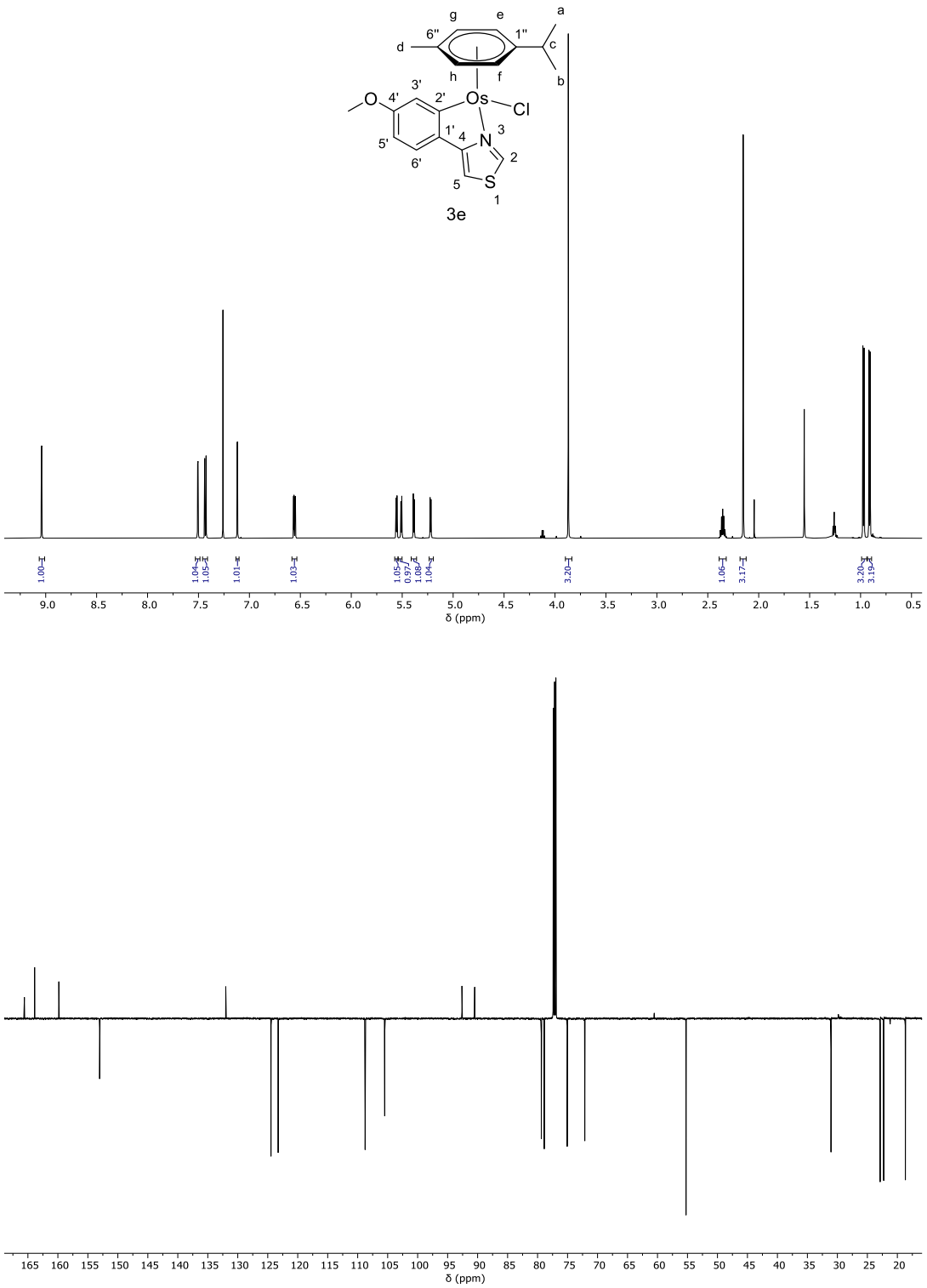

Figure S15: Atom numbering (above), ^{1}H (center) and ^{13}C (below) NMR of **3e** in $CDCl_3$.

3. Mass spectra

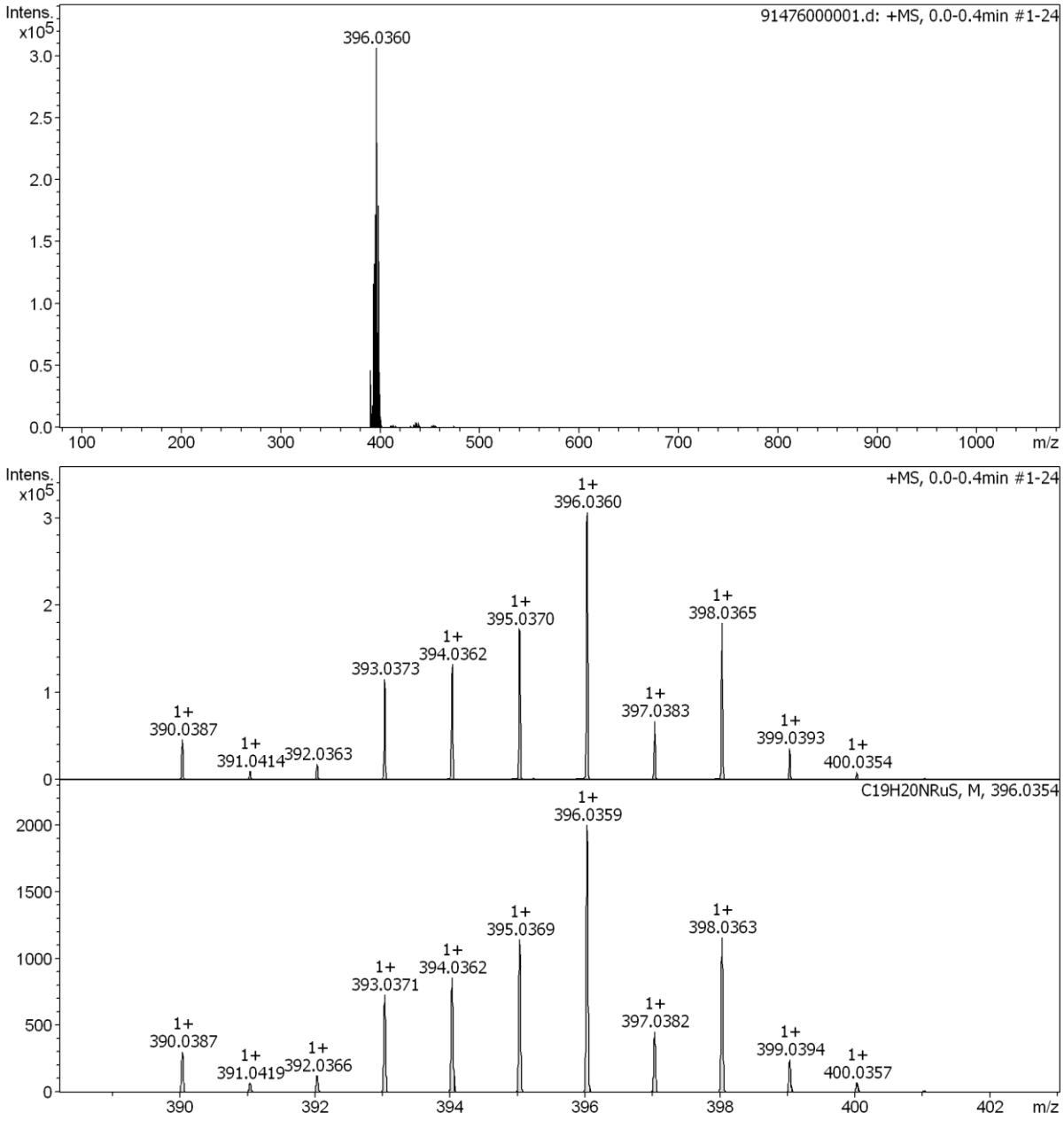

Figure S16: Top and middle: Mass spectrum of **2a** $(M\text{-}Cl)^+$; Bottom: Calculated mass spectrum of **2a** $(M\text{-}Cl)^+$.

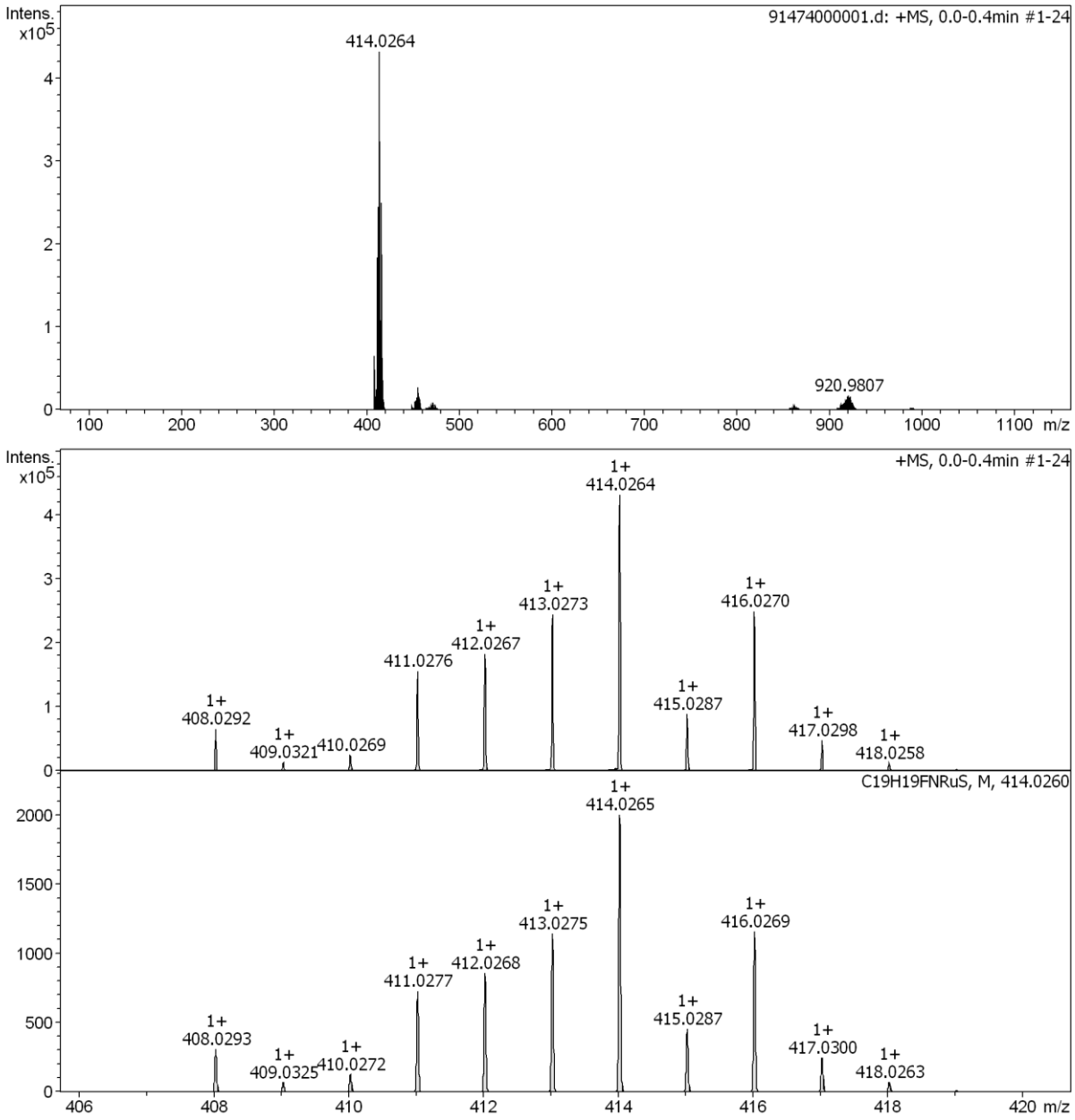

Figure S17: Top and middle: Mass spectrum of **2b** $(M\text{-}Cl)^+$; Bottom: Calculated mass spectrum of **2b** $(M\text{-}Cl)^+$.

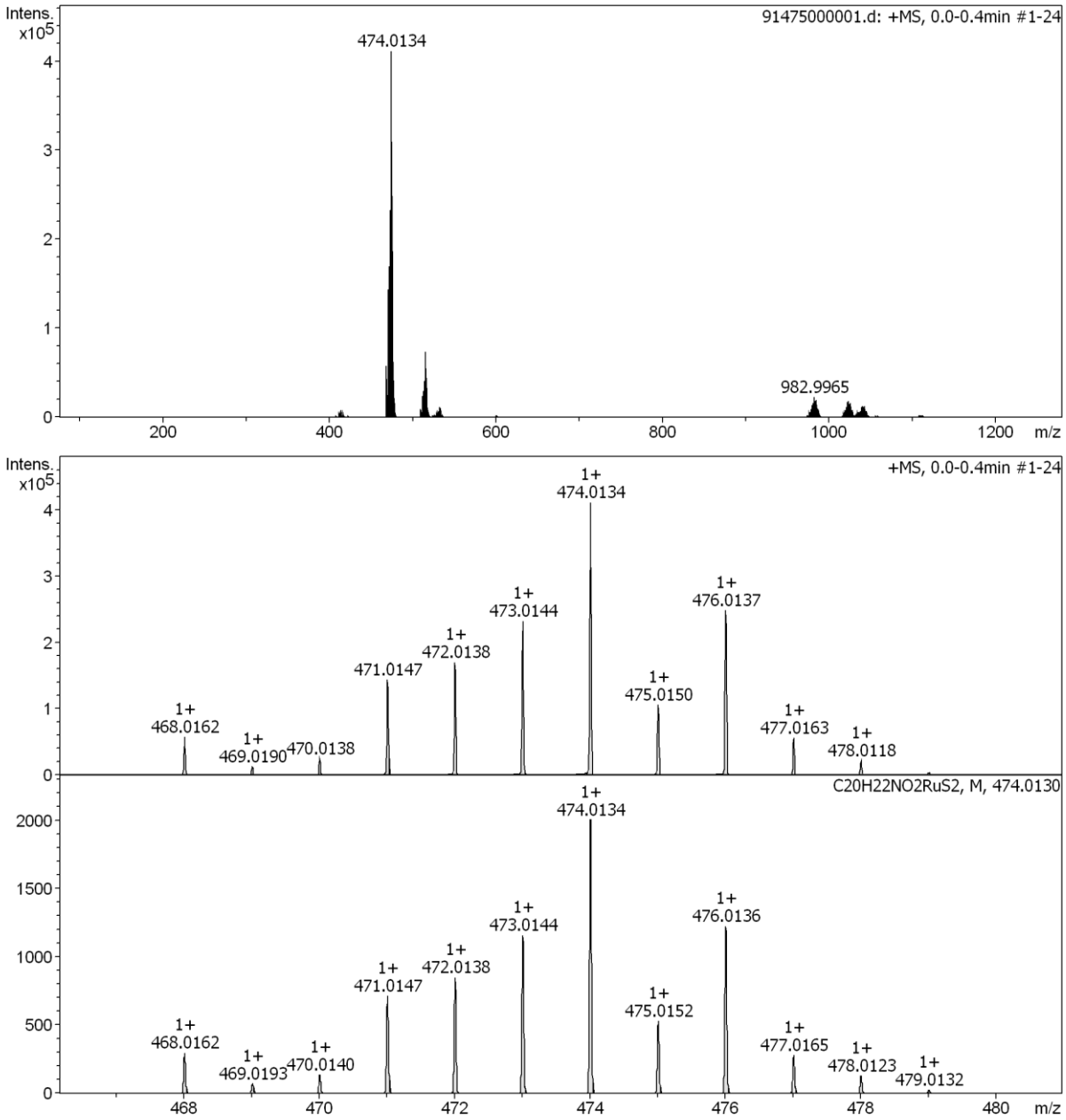

Figure S18: Top and middle: Mass spectrum of **2c** $(M\text{-}Cl)^+$; Bottom: Calculated mass spectrum of **2c** $(M\text{-}Cl)^+$.

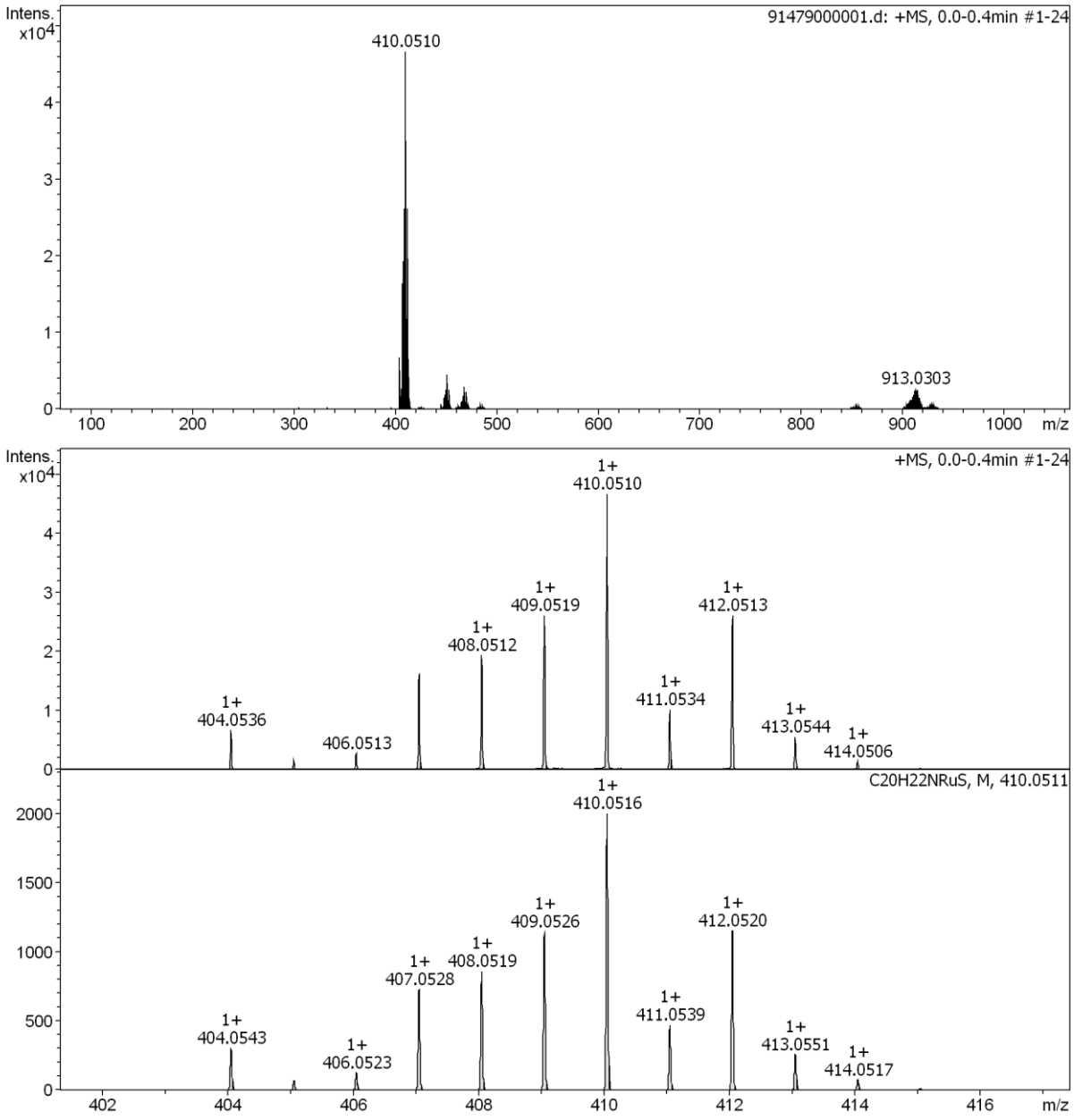

Figure S19: Top and middle: Mass spectrum of **2d** $(M\text{-}Cl)^+$; Bottom: Calculated mass spectrum of **2d** $(M\text{-}Cl)^+$.

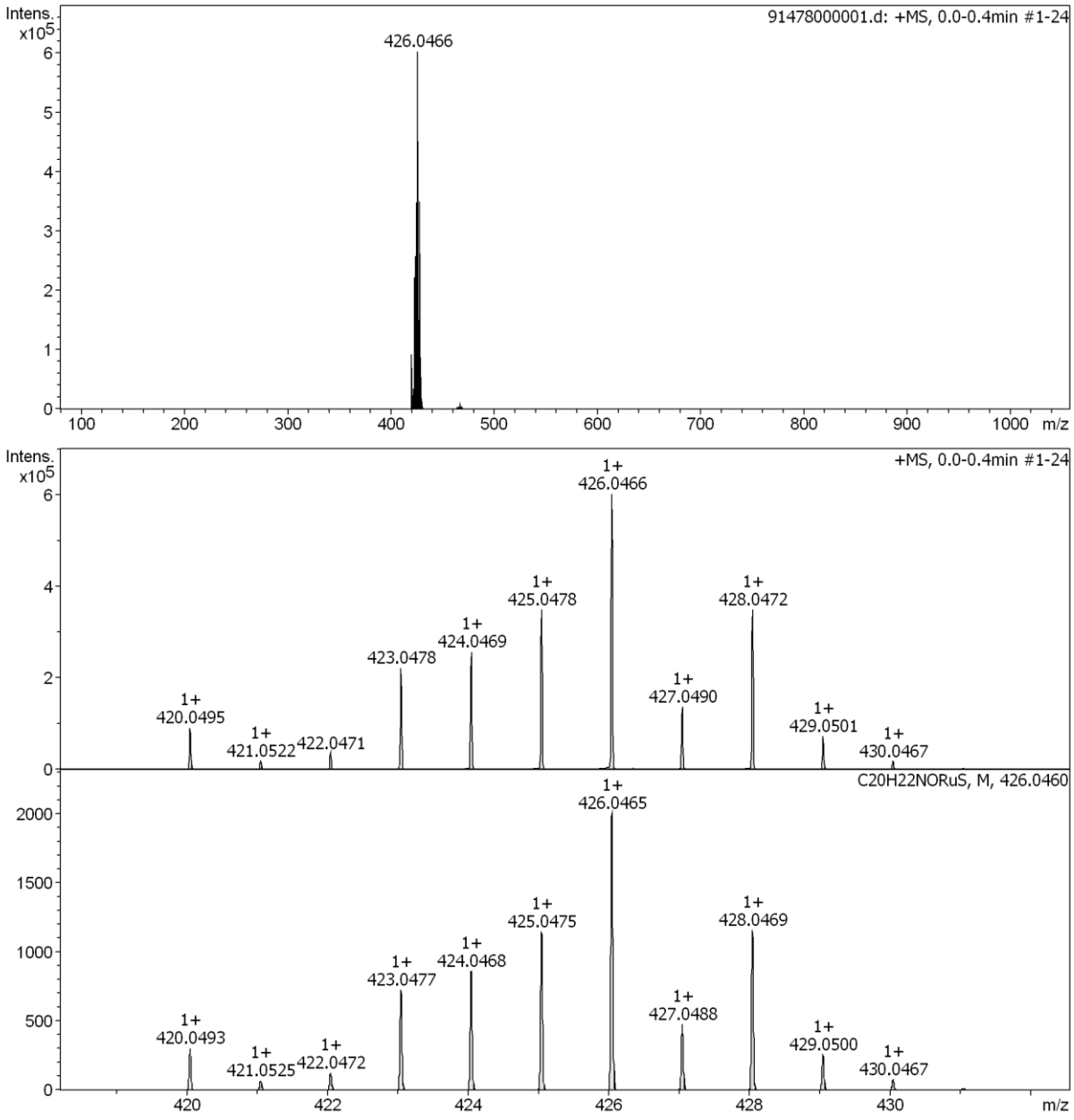

Figure S20: Top and middle: Mass spectrum of **2e** $(M\text{-}Cl)^+$; Bottom: Calculated mass spectrum of **2e** $(M\text{-}Cl)^+$.

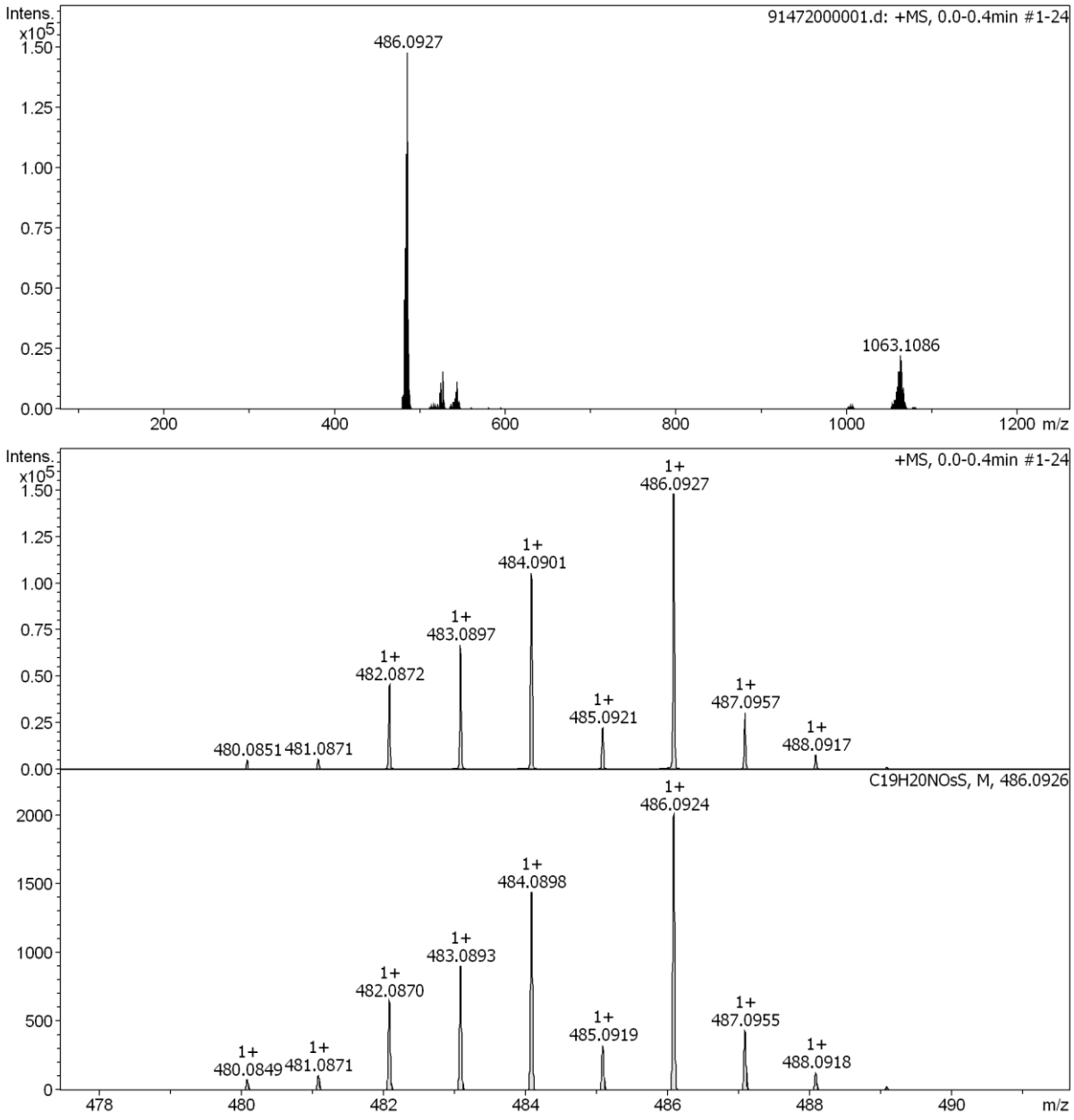

Figure S21: Top and middle: Mass spectrum of **3a** $(M\text{-}Cl)^+$; Bottom: Calculated mass spectrum of **3a** $(M\text{-}Cl)^+$.

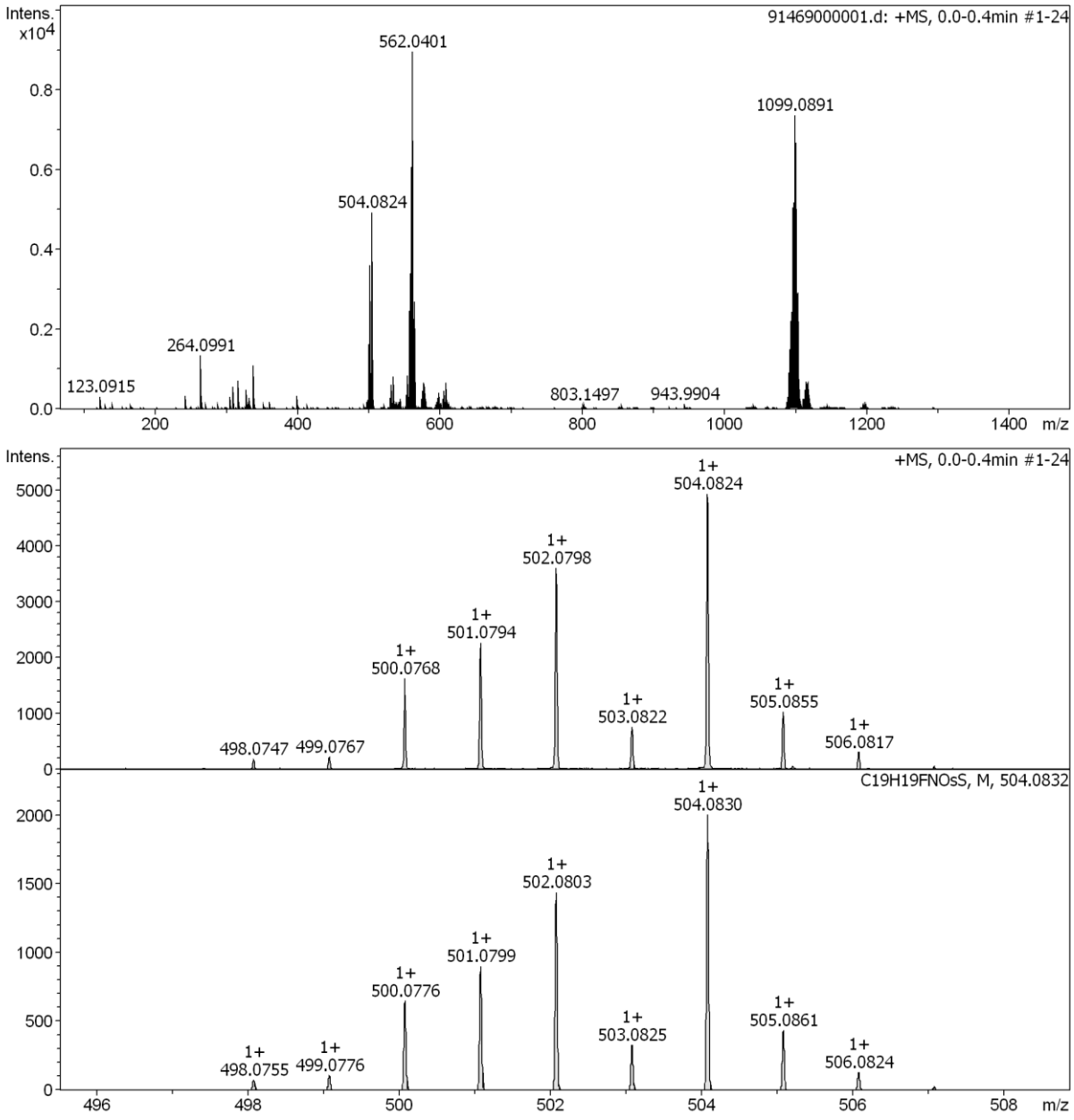

Figure S22: Top and middle: Mass spectrum of **3b** $(M\text{-}Cl)^+$; Bottom: Calculated mass spectrum of **3b** $(M\text{-}Cl)^+$.

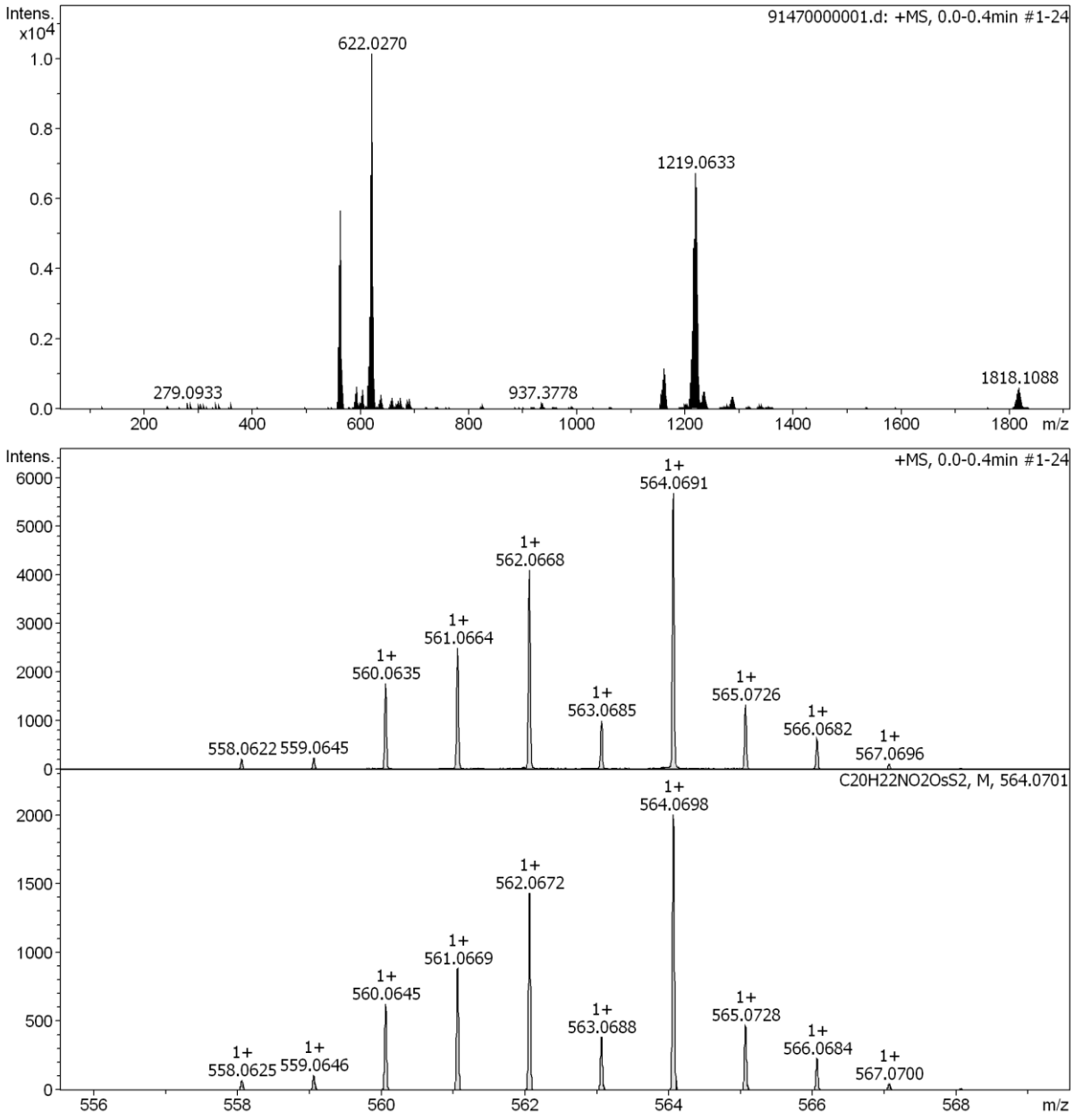

Figure S23: Top and middle: Mass spectrum of **3c** $(M\text{-}Cl)^+$; Bottom: Calculated mass spectrum of **3c** $(M\text{-}Cl)^+$.

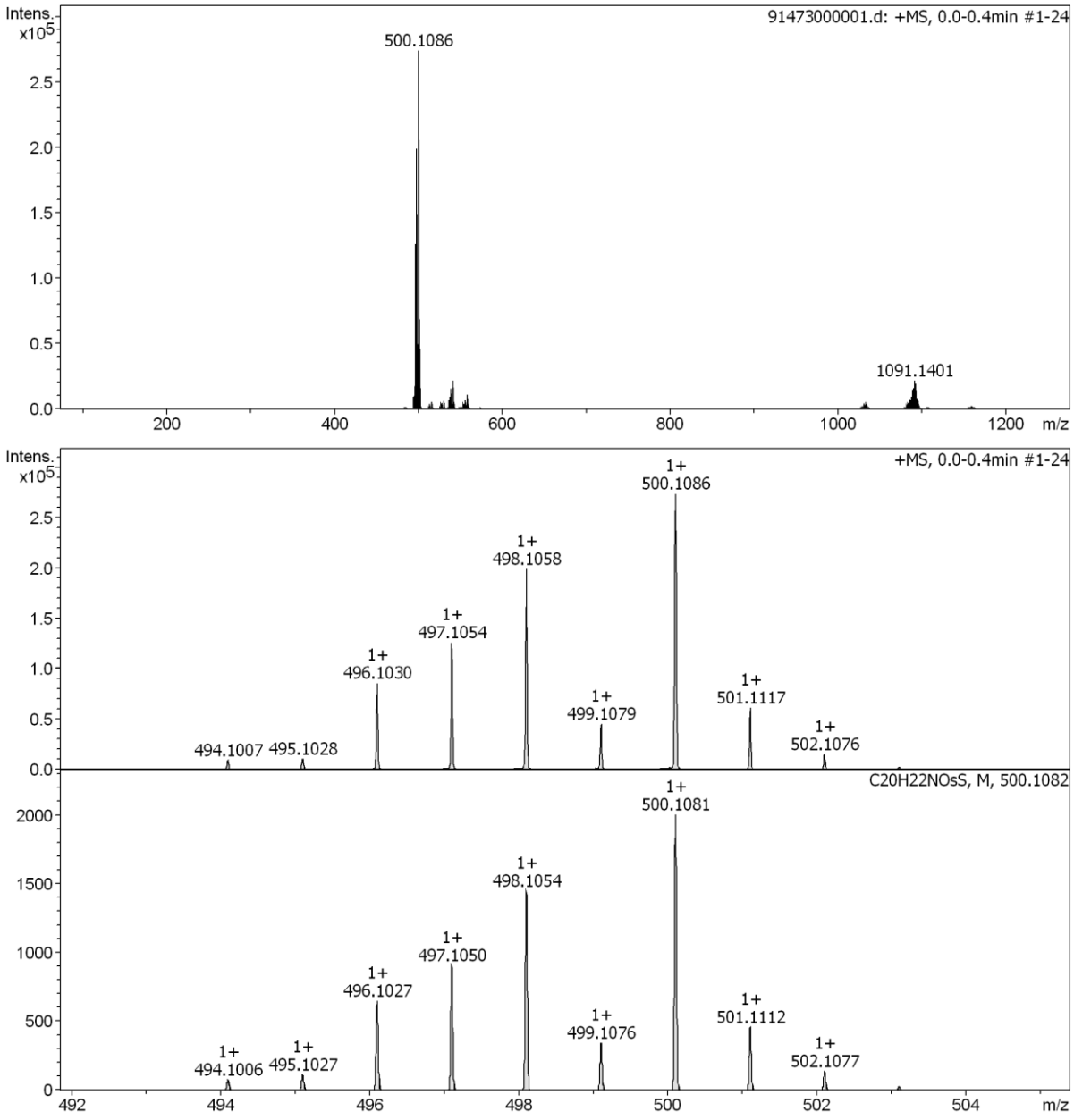

Figure S24: Top and middle: Mass spectrum of **3d** $(M\text{-}Cl)^+$; Bottom: Calculated mass spectrum of **3d** $(M\text{-}Cl)^+$.

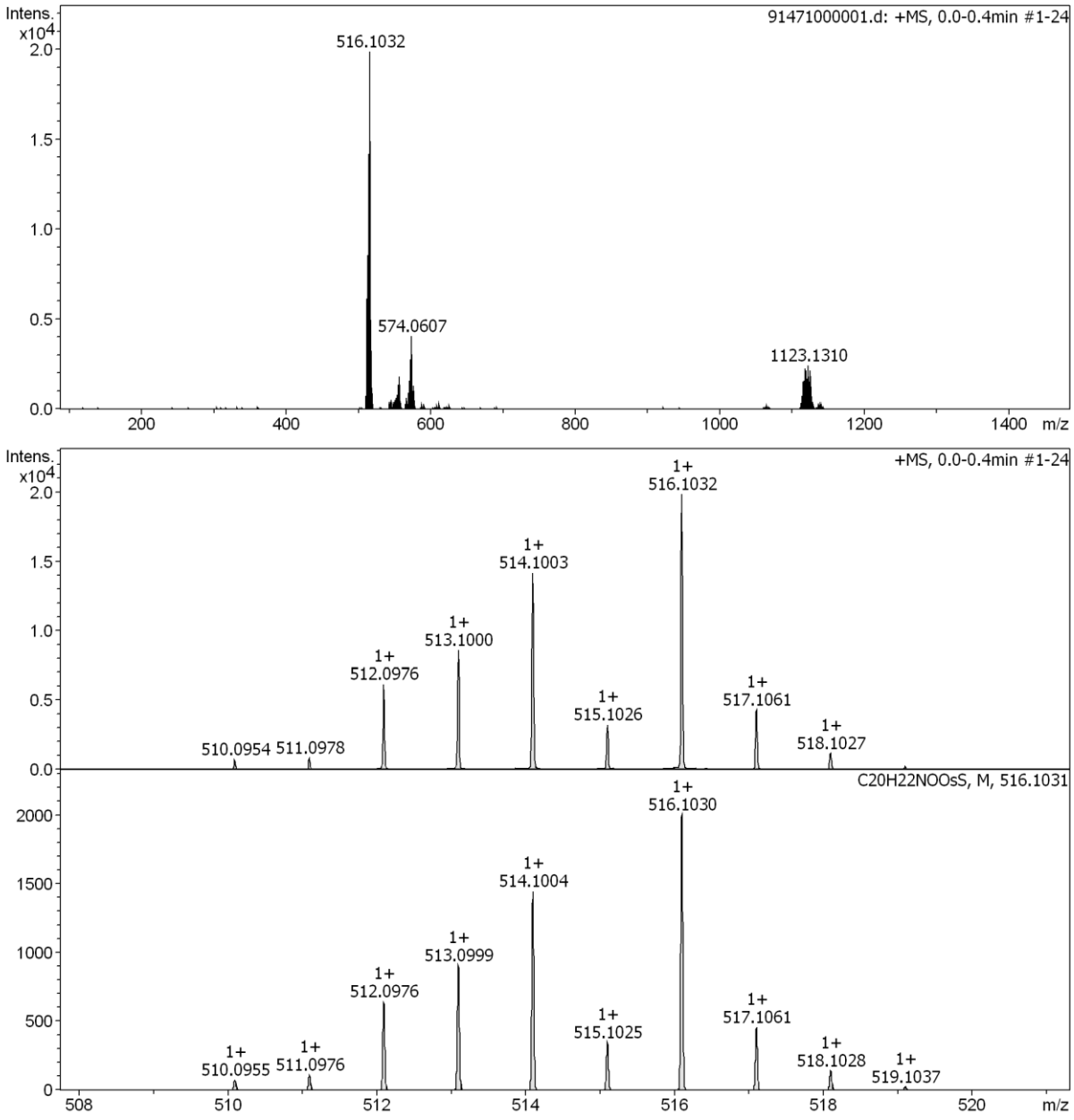

Figure S25: Top and middle: Mass spectrum of **3e** $(M\text{-}Cl)^+$; Bottom: Calculated mass spectrum of **3e** $(M\text{-}Cl)^+$.

4. X-ray diffraction analysis

The X-ray intensity data were measured on STOE STADIVARI diffractometer equipped with multilayer monochromator, micro focus sealed tube and Oxford cooling system (Cu K/α mit Primux 100 micro, Mo K/α mit AXO Mo). The structures were solved by *Intrinsic Phasing, Charge Flipping or Direct Methods*. Non-hydrogen atoms were refined with *anisotropic displacement parameters*. Hydrogen atoms were inserted at calculated positions and refined with riding model. The following software was used: X-Area Recipe[i], *X-Area Pilatus3_SV*[ii], *OLEX2*[iii] for cell refinement, data collection, molecular diagrams and graphical user-interface, *SHELXLE*[iv] for refinement and graphical user-interface *SHELXT-2015*[v] for structure solution, *SHELXL-2015*[vi] for refinement, *Platon*[vii] for symmetry check. Experimental data and CCDC-Codes Experimental data (Available online: http://www.ccdc.cam.ac.uk/conts/retrieving.html) can be found in Table S1. Crystal data, data collection parameters, and structure refinement details are reported in Tables S2 to S8. Structures, packing, interactions, and data are visualized in Figures S1 to S8.

Table S1: Experimental Parameters and CCDC codes. Responsible for data evaluation: A. Prado-Roller.

Sample	Machine	Source	Temp.	Detector distance	Time/ Frame	#Frames	Frame width	CCDC
			[K]	[mm]	[s]		[°]	
2a	Stoe	Mo	100	50	0.1	2282	0.4	2296750
2b	Stoe	Mo	100	50	0.5	3063	0.4	2296747
2d	Stoe	Cu	100	40	1	14164	0.5	2296751
2e	Stoe	Mo	100	50	0.1	2472	0.4	2296753
3a	Stoe	Mo	100	40	4	3175	0.5	2296749
3b	Stoe	Mo	100	50	0.5	4647	0.4	2296745
3d	Stoe	Mo	100	40	2	2804	0.5	2296746

[i] Version 1.37.0.0 (STOE, 2021)

[ii] Version 1.31.186.0 (STOE, 2022)

[iii] Dolomanov, O.V., Bourhis, L.J., Gildea, R.J, Howard, J.A.K. & Puschmann, H., OLEX2, (2009), J. Appl. Cryst. 42, 339-341

[iv] C. B. Huebschle, G. M. Sheldrick and B. Dittrich, ShelXle: a Qt graphical user interface for SHELXL, J. Appl. Cryst., 44, (2011) 1281-1284

[v] Sheldrick, G. M. (2015). *SHELXS v 2016/4* University of Göttingen, Germany.

[vi] Sheldrick, G. M. (2015). *SHELXL v 2016/4* University of Göttingen, Germany.

[vii] A. L. Spek, Acta Cryst. 2009, D65, 148-155

[(Chlorido)(4-phenylthiazolato-κN,κC2´)(η^6-*p*-cymene)ruthenium(II)] (2a)

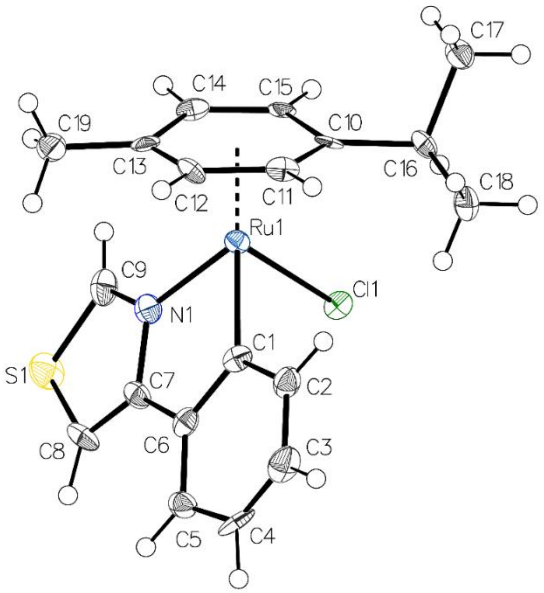

Figure S26: Crystal structure of **2a**, depicted using 50% displacement ellipsoids.

Table S2: Crystal data and structure refinement of **2a**.

Chemical formula	$C_{19}H_{20}ClNRuS$
Formula weight [g/mol]	430.94
Temperature [°K]	100
Crystal system	monoclinic
Space group	$P2_{1/n}$
a [Å]	7.9520(17)
b [Å]	12.1531(12)
c [Å]	18.037(3)
α [°]	90
β [°]	99.698(15)
γ [°]	90
Volume [Å]	1718.2(5)
Z	4
Density (calc.) [g/cm$^{3]}$	1.666
Absorption coeff. [mm^{-1}]	1.187
F(000)	872.0
Crystal size [mm]	0.5 × 0.32 × 0.16

Crystal habit	Orange block
Radiation wavelength	Mo Kα (λ = 0.71073)
2Θ range for data collection [°]	4.06 to 50.694
Index ranges	-9 ≤ h ≤ 9, -14 ≤ k ≤ 14, -21 ≤ l ≤ 20
Reflections collected	16878
Independent reflections	3149 [R_{int} = 0.0787, R_{sigma} = 0.0704]
Data/restraints/ parameters	3149/0/211
Goodness-of-fit on F	0.992
Final R indexes [I≥2σ (I)]	R_1 = 0.0504, wR_2 = 0.1180
Final R indexes [all data]	R_1 = 0.0658, wR_2 = 0.1284
Largest diff. peak/hole [Å]	1.18/-1.50

[(Chlorido)(4-(4-fluorophenyl)thiazolato-κN,κC2´)(η^6-*p*-cymene)ruthenium(II)] (2b)

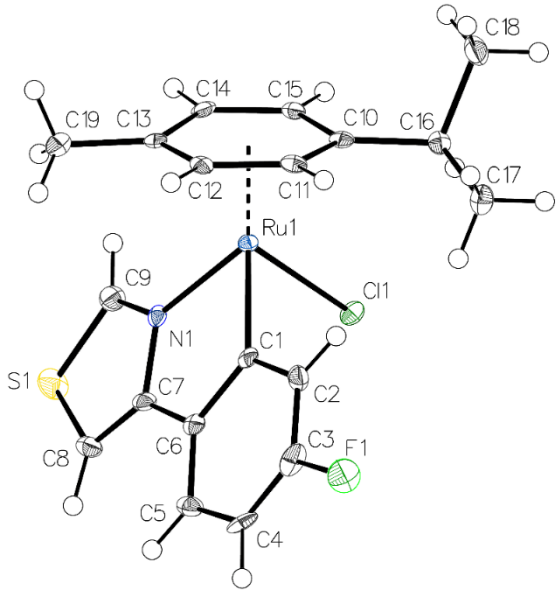

Figure S27: Crystal structure of **2b**, depicted with 50% displacement ellipsoids.

Table S3: Crystal data and structure refinement of **2b**.

Chemical formula	$C_{19}H_{19}ClFNRuS$
Formula weight [g/mol]	448.93
Temperature [°K]	100
Crystal system	monoclinic
Space group	$P2_{1/n}$
a [Å]	7.8645(8)
b [Å]	12.1266(14)
c [Å]	18.5026(17)
α [°]	90
β [°]	99.203(8)
γ [°]	90
Volume [Å]	1741.9(3)
Z	4
Density (calc.) [g/cm^3]	1.712
Absorption coeff. [mm^{-1}]	1.183
F(000)	904.0
Crystal size [mm]	0.13 × 0.12 × 0.1
Crystal habit	Yellow chunk

Radiation wavelength	Mo Kα (λ = 0.71073)
2Θ range for data collection [°]	4.032 to 61.978
Index ranges	-11 ≤ h ≤ 11, -17 ≤ k ≤ 17, -26 ≤ l ≤ 26
Reflections collected	48483
Independent reflections	5302 [R_{int} = 0.0540, R_{sigma} = 0.0919]
Data/restraints/ parameters	5302/0/220
Goodness-of-fit on F	0.896
Final R indexes [I≥2σ (I)]	R_1 = 0.0271, wR_2 = 0.0482
Final R indexes [all data]	R_1 = 0.0489, wR_2 = 0.0507
Largest diff. peak/hole [Å]	0.85/-1.73

Water cocrystal structure available (CCDC code: 2296748).

[(Chlorido)(4-(4-methylphenyl)thiazolato-κN,κC2´)(η^6-*p*-cymene)ruthenium(II)] (2d)

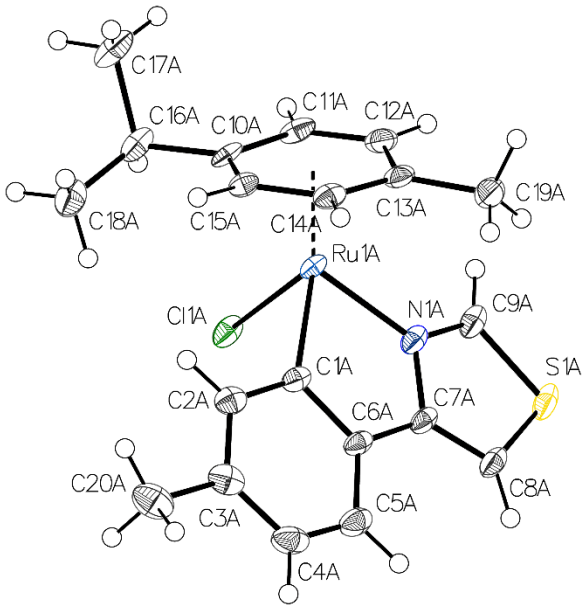

Figure S28: Crystal structure of **2d**, depicted with 50% displacement ellipsoids. The second molecule of the asymmetric unit is not shown for clarity reasons.

Table S4: Crystal data and structure refinement of **2d**.

Chemical formula	$C_{20}H_{22}ClNRuS$
Formula weight [g/mol]	444.96
Temperature [°K]	100
Crystal system	monoclinic
Space group	$P2_{1/c}$
a [Å]	19.8899(2)
b [Å]	12.5816(1)
c [Å]	14.901(2)
α [°]	90
β [°]	96.418(10)
γ [°]	90
Volume [Å]	3705.56(7)
Z	8
Density (calc.) [g/cm$^{3]}$	1.595
Absorption coeff. [mm^{-1}]	9.218
F(000)	1808.0
Crystal size [mm]	0.244 × 0.174 × 0.117

Crystal habit	Orange chunk
Radiation wavelength	Cu Kα (λ = 1.54178)
2Θ range for data collection [°]	8.33 to 139.892
Index ranges	-24 ≤ h ≤ 21, -15 ≤ k ≤ 14, -18 ≤ l ≤ 8
Reflections collected	79338
Independent reflections	6746 [R_{int} = 0.019, R_{sigma} = 0.0083]
Data/restraints/ parameters	6746/0/442
Goodness-of-fit on F	1.087
Final R indexes [I≥2σ (I)]	R_1 = 0.0296, wR_2 = 0.0783
Final R indexes [all data]	R_1 = 0.0305, wR_2 = 0.0789
Largest diff. peak/hole [Å]	1.5/-1.5

[(Chlorido)(4-(4-methoxyphenyl)thiazolato-κN,κC2´)(η^6-*p*-cymene)ruthenium(II)] (2e)

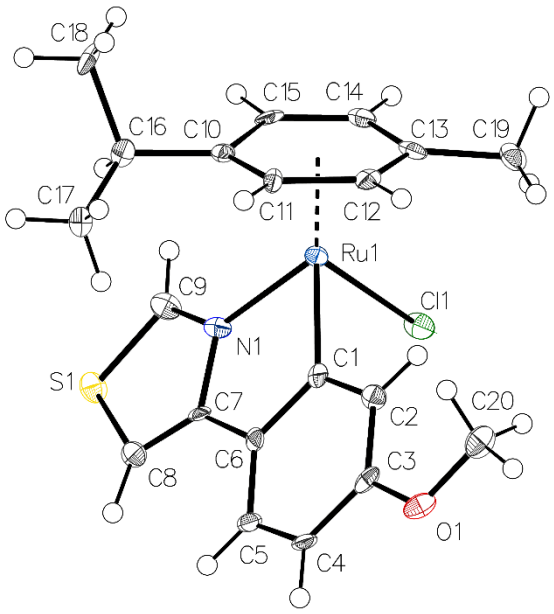

Figure S29: Crystal structure of **2e**, depicted with 50% displacement ellipsoids.

Table S5: Crystal data and structure refinement of **2e**.

Chemical formula	$C_{20}H_{22}ClNORuS$
Formula weight [g/mol]	460.96
Temperature [°K]	100
Crystal system	monoclinic
Space group	$P2_{1/n}$
a [Å]	14.523(2)
b [Å]	9.328(2)
c [Å]	14.748(2)
α [°]	90
β [°]	107.171(11)
γ [°]	90
Volume [Å]	1908.9(6)
Z	4
Density (calc.) [g/cm^3]	1.604
Absorption coeff. [mm^{-1}]	1.078
F(000)	936.0
Crystal size [mm]	0.3 × 0.267 × 0.25

Crystal habit	Orange chunk
Radiation wavelength	Mo Kα (λ = 0.71073)
2Θ range for data collection [°]	3.458 to 50.698
Index ranges	-17 ≤ h ≤ 17, -11 ≤ k ≤ 9, -17 ≤ l ≤ 17
Reflections collected	16385
Independent reflections	3492 [R_{int} = 0.0613, R_{sigma} = 0.0967]
Data/restraints/ parameters	3492/0/230
Goodness-of-fit on F	0.849
Final R indexes [I≥2σ (I)]	R_1 = 0.0340, wR_2 = 0.0632
Final R indexes [all data]	R_1 = 0.0513, wR_2 = 0.0664
Largest diff. peak/hole [Å]	0.64/-0.92

(Chlorido)(4-phenylthiazolato-κN,κC2´)(η^6-*p*-cymene)osmium(II)] (3a)

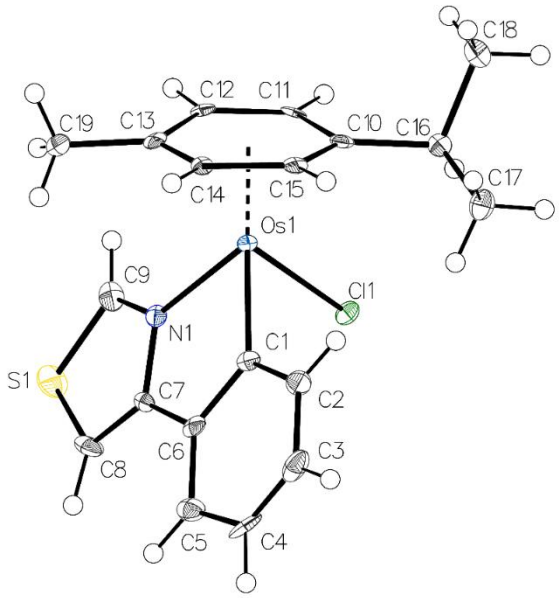

Figure S30: Crystal structure of **3a**, depicted with 50% displacement ellipsoids.

Table S6: Crystal data and structure refinement of **3a**.

Chemical formula	$C_{19}H_{20}ClNOsS$
Formula weight [g/mol]	520.07
Temperature [°K]	100
Crystal system	monoclinic
Space group	$P2_{1/n}$
a [Å]	7.9442(3)
b [Å]	12.0992(4)
c [Å]	18.0987(6)
α [°]	90
β [°]	99.821(3)
γ [°]	90
Volume [Å]	1714.13(10)
Z	4
Density (calc.) [g/cm$^{3]}$	2.015
Absorption coeff. [mm^{-1}]	7.715
F(000)	1000.0
Crystal size [mm]	0.08 × 0.08 × 0.08

Crystal habit	Yellow chunk
Radiation wavelength	Mo Kα (λ = 0.71073)
2Θ range for data collection [°]	5.314 to 57.31
Index ranges	-10 ≤ h ≤ 10, -15 ≤ k ≤ 16, -21 ≤ l ≤ 24
Reflections collected	37949
Independent reflections	4268 [R_{int} = 0.0578, R_{sigma} = 0.0443]
Data/restraints/ parameters	4268/0/211
Goodness-of-fit on F	1.038
Final R indexes [I≥2σ (I)]	R_1 = 0.0248, wR_2 = 0.0511
Final R indexes [all data]	R_1 = 0.0420, wR_2 = 0.0569
Largest diff. peak/hole [Å]	1.52/-2.02

(Chlorido)(4-(4-fluorophenyl)thiazolato-κN,κC2´)(η^6-*p*-cymene)osmium(II)] (3b)

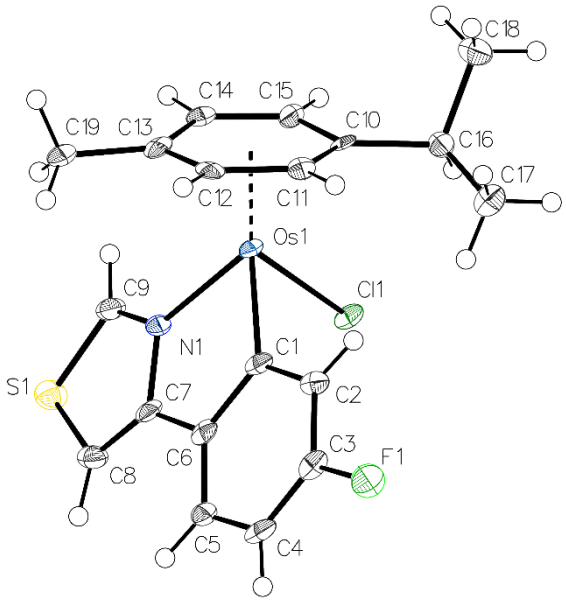

Figure S31: Crystal structure of **3b**, depicted with 50% displacement ellipsoids.

Table S7: Crystal data and structure refinement of **3b**.

Chemical formula	$C_{19}H_{19}ClFNOsS$
Formula weight [g/mol]	538.06
Temperature [°K]	100
Crystal system	monoclinic
Space group	$P2_{1/n}$
a [Å]	7.8664(6)
b [Å]	12.0681(12)
c [Å]	18.5613(15)
α [°]	90
β [°]	99.276(6)
γ [°]	90
Volume [Å]	1739.0(3)
Z	4
Density (calc.) [g/cm$^{3]}$	2.055
Absorption coeff. [mm^{-1}]	7.616
F(000)	1032.0
Crystal size [mm]	0.24 × 0.22 × 0.2

Crystal habit	Yellow chunk
Radiation wavelength	Mo Kα (λ = 0.71073)
2Θ range for data collection [°]	4.042 to 50.692
Index ranges	-9 ≤ h ≤ 9, -14 ≤ k ≤ 14, -22 ≤ l ≤ 22
Reflections collected	32861
Independent reflections	3193 [R_{int} = 0.0969, R_{sigma} = 0.0500]
Data/restraints/ parameters	3193/0/221
Goodness-of-fit on F	1.006
Final R indexes [I≥2σ (I)]	R_1 = 0.0383, wR_2 = 0.0949
Final R indexes [all data]	R_1 = 0.0519, wR_2 = 0.1019
Largest diff. peak/hole [Å]	2.21/-2.33

Water cocrystal structure available (CCDC code: 2296752).

(Chlorido)(4-(4-methylphenyl)thiazolato-κN,κC2´)(η^6-*p*-cymene)osmium(II)] (3d)

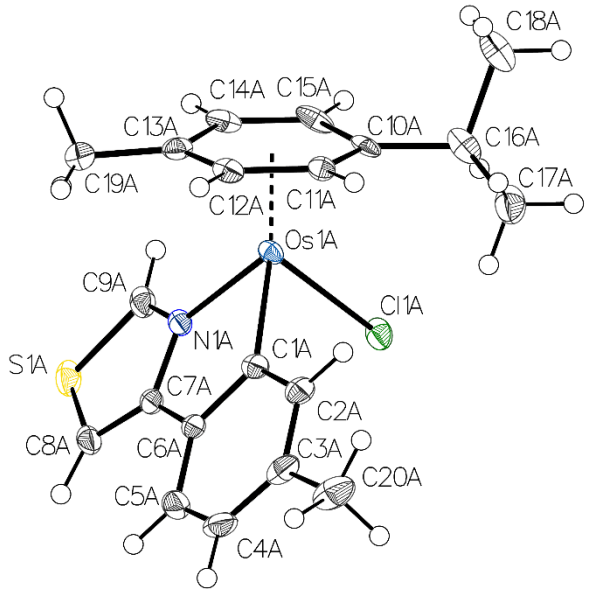

Figure S32: Crystal structure of **3d**, depicted with 50% displacement ellipsoids. The second molecule of the asymmetric unit is not shown for clarity reasons.

Table S8: Crystal data and structure refinement of **3d**.

Chemical formula	$C_{20}H_{22}ClNOsS$
Formula weight [g/mol]	534.09
Temperature [°K]	100
Crystal system	monoclinic
Space group	$P2_{1/c}$
a [Å]	19.8295(5)
b [Å]	12.5808(2)
c [Å]	14.9234(3)
α [°]	90
β [°]	95.974(2)
γ [°]	90
Volume [Å]	3702.74(13)
Z	8
Density (calc.) [g/cm$^{3]}$	1.916
Absorption coeff. [mm^{-1}]	7.146
F(000)	2064.0
Crystal size [mm]	0.22 × 0.133 × 0.08

Crystal Habit	Yellow chunk
Radiation wavelength	Mo Kα (λ = 0.71073)
2Θ range for data collection [°]	4.244 to 60.066
Index ranges	-27 ≤ h ≤ 27, -17 ≤ k ≤ 14, -20 ≤ l ≤ 20
Reflections collected	83084
Independent reflections	10822 [R_{int} = 0.0507, R_{sigma} = 0.0532]
Data/restraints/ parameters	10822/0/462
Goodness-of-fit on F	0.931
Final R indexes [I≥2σ (I)]	R_1 = 0.0240, wR_2 = 0.0396
Final R indexes [all data]	R_1 = 0.0416, wR_2 = 0.0410
Largest diff. peak/hole [Å]	2.41/-1.42

5. Stability in aqueous solution

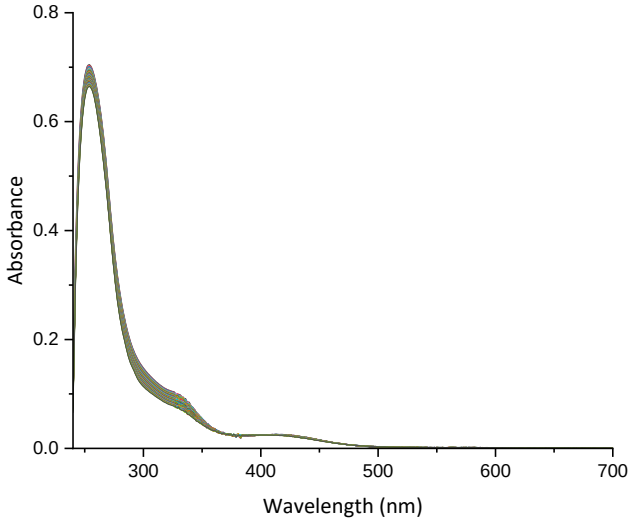

Figure S33: UV-Vis spectra of **2a** in PBS (1% DMF), 30 min intervals over 24 h.

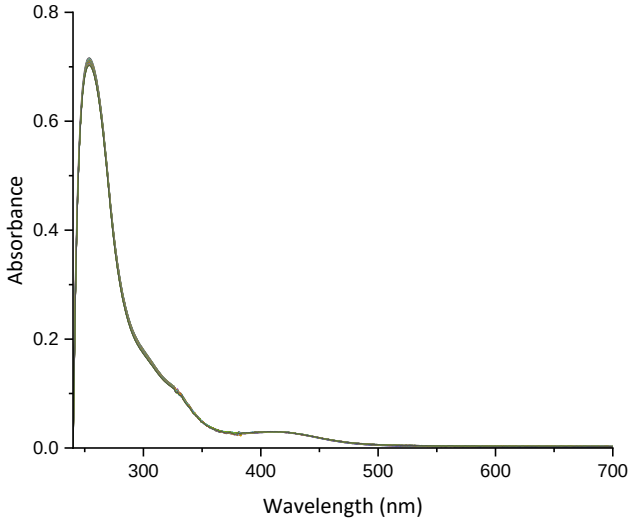

Figure S34: UV-Vis spectra of **2b** in PBS (1% DMF), 30 min intervals over 24 h.

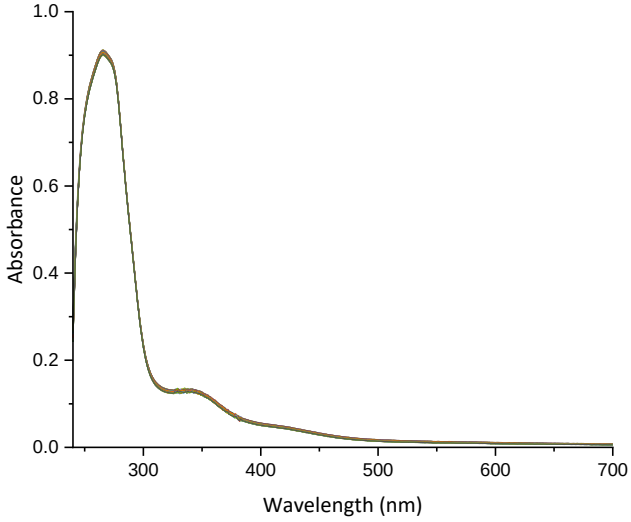

Figure S35: UV-Vis spectra of **2c** in PBS (1% DMF), 30 min intervals over 24 h.

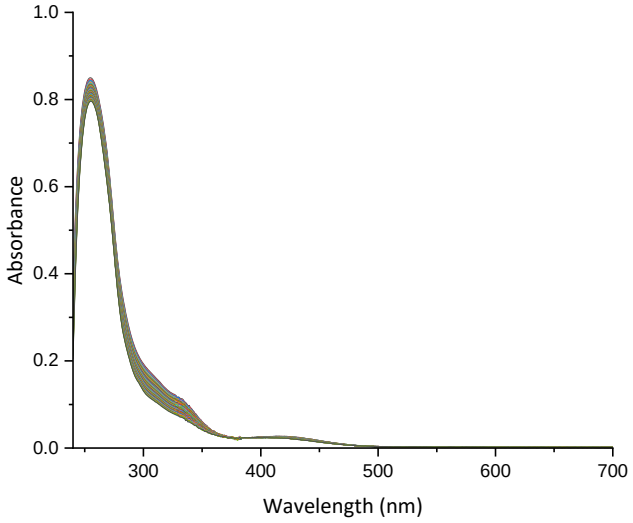

Figure S36: UV-Vis spectra of **2d** in PBS (1% DMF), 30 min intervals over 24 h.

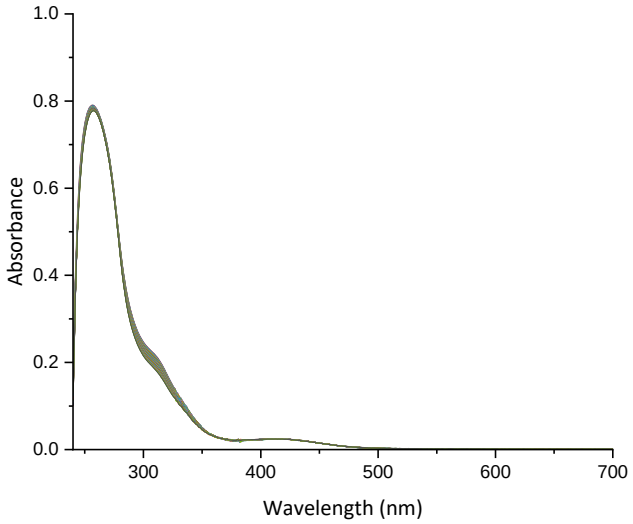

Figure S37: UV-Vis spectra of **2e** in PBS (1% DMF), 30 min intervals over 24 h.

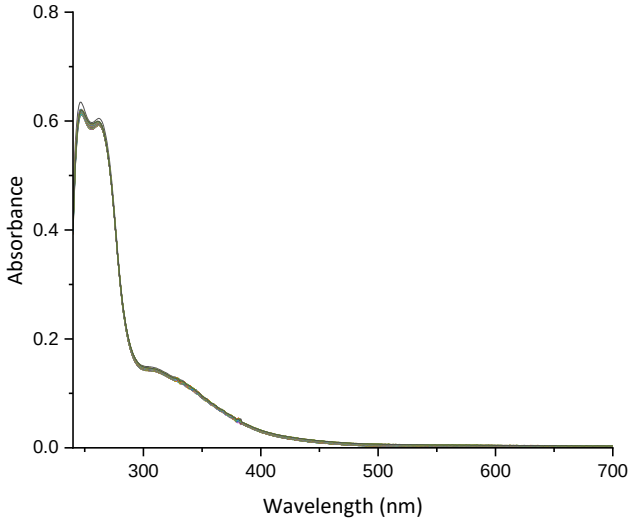

Figure S38: UV-Vis spectra of **3a** in PBS (1% DMF), 30 min intervals over 24 h.

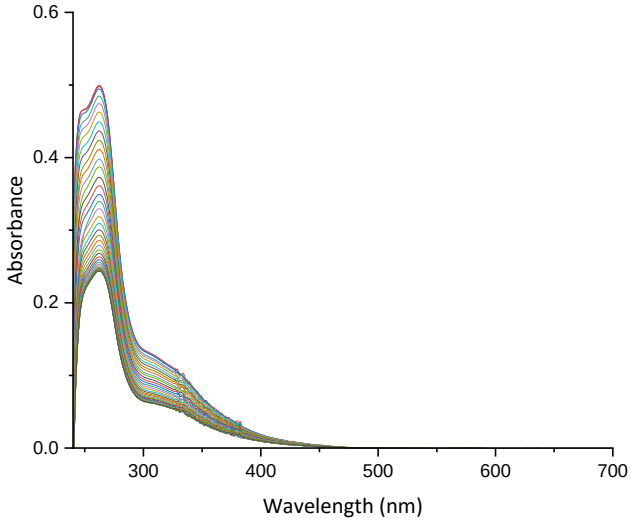

Figure S39: UV-Vis spectra of **3b** in PBS (1% DMF), 30 min intervals over 24 h.

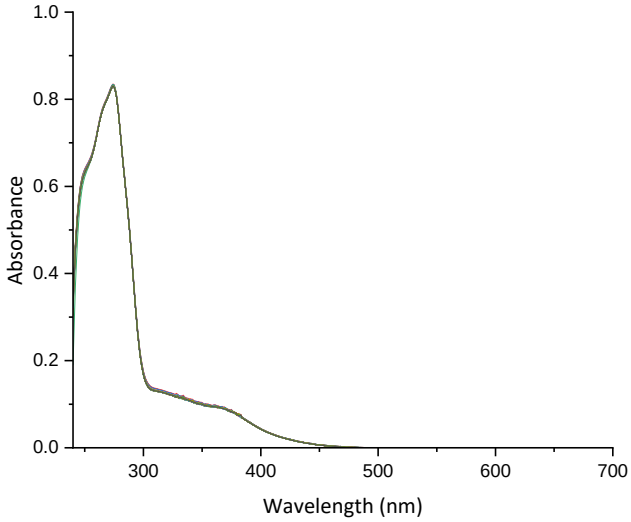

Figure S40: UV-Vis spectra of **3c** in PBS (1% DMF), 30 min intervals over 24 h.

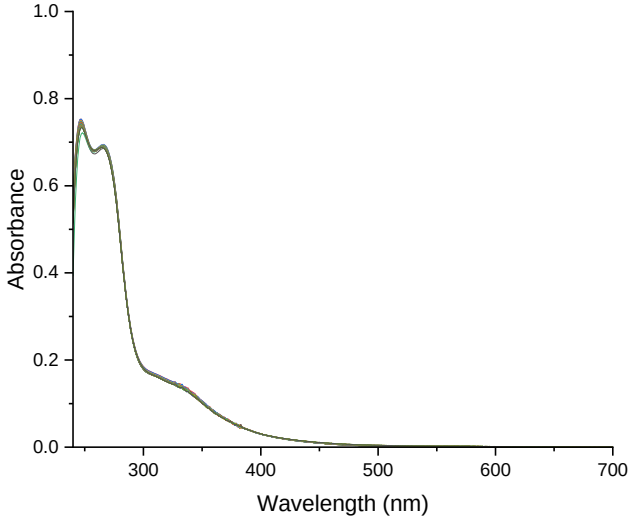

Figure S41: UV-Vis spectra of **3d** in PBS (1% DMF), 30 min intervals over 24 h.

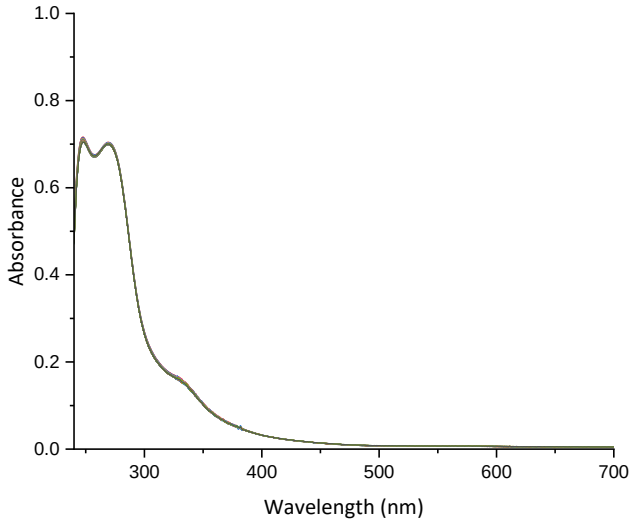

Figure S42: UV-Vis spectra of **3e** in PBS (1% DMF), 30 min intervals over 24 h.

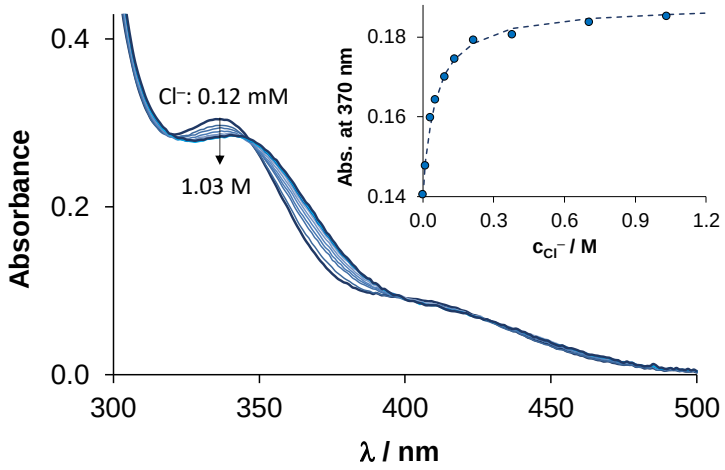

Figure S43: UV-vis absorption spectra of **2c** at various chloride ion (KCl) concentrations. Inserted figure shows the changes of absorbance at 370 nm {$c_{complex}$ = 120 µM; pH 7.4 (20 mM phosphate, 1% DMF); 25 °C}.

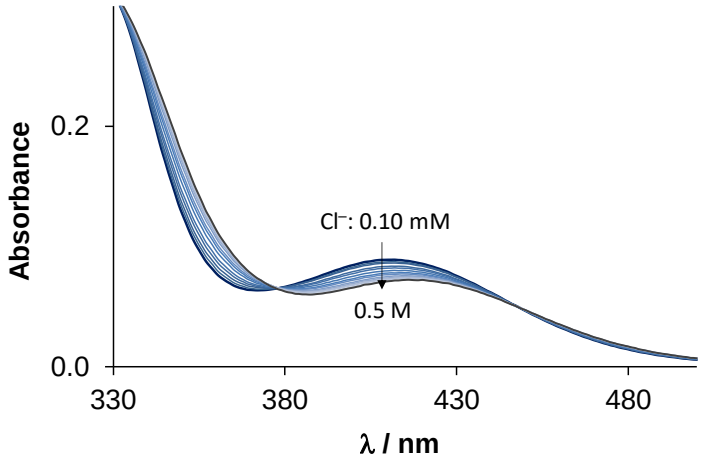

Figure S44: UV-vis absorption spectra of **2a** at various chloride ion (KCl) concentrations. {$c_{complex}$ = 102 µM; pH 7.4 (20 mM phosphate, 1% DMF); 25 °C}.

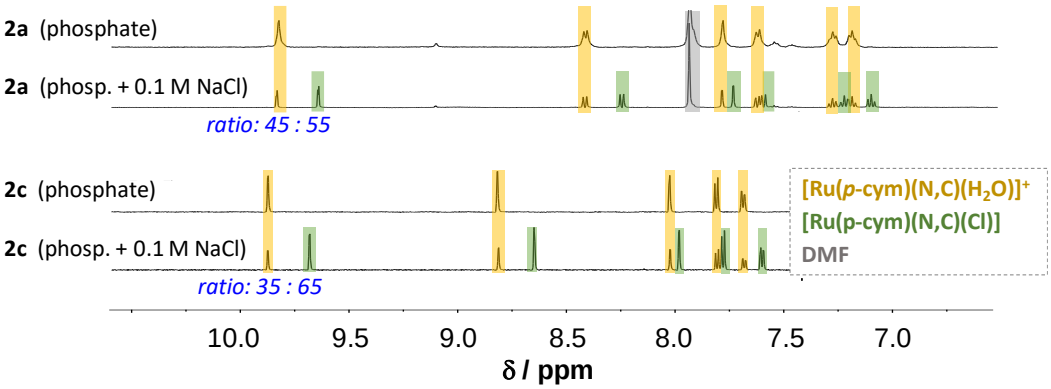

Figure S45: ^{1}H NMR spectra of **2a** and **2c** at pH 7.4 prepared in 20 mM phosphate buffer and in phosphate buffer containing 0.1 M NaCl and recorded after 15 min. {$c_{complex}$ = 1 mM; samples of **2a** contained 10%(v/v) DMF-d^7; **2c** contained 10%(v/v) D_2O; 25 °C}.

6. MTT-Assays

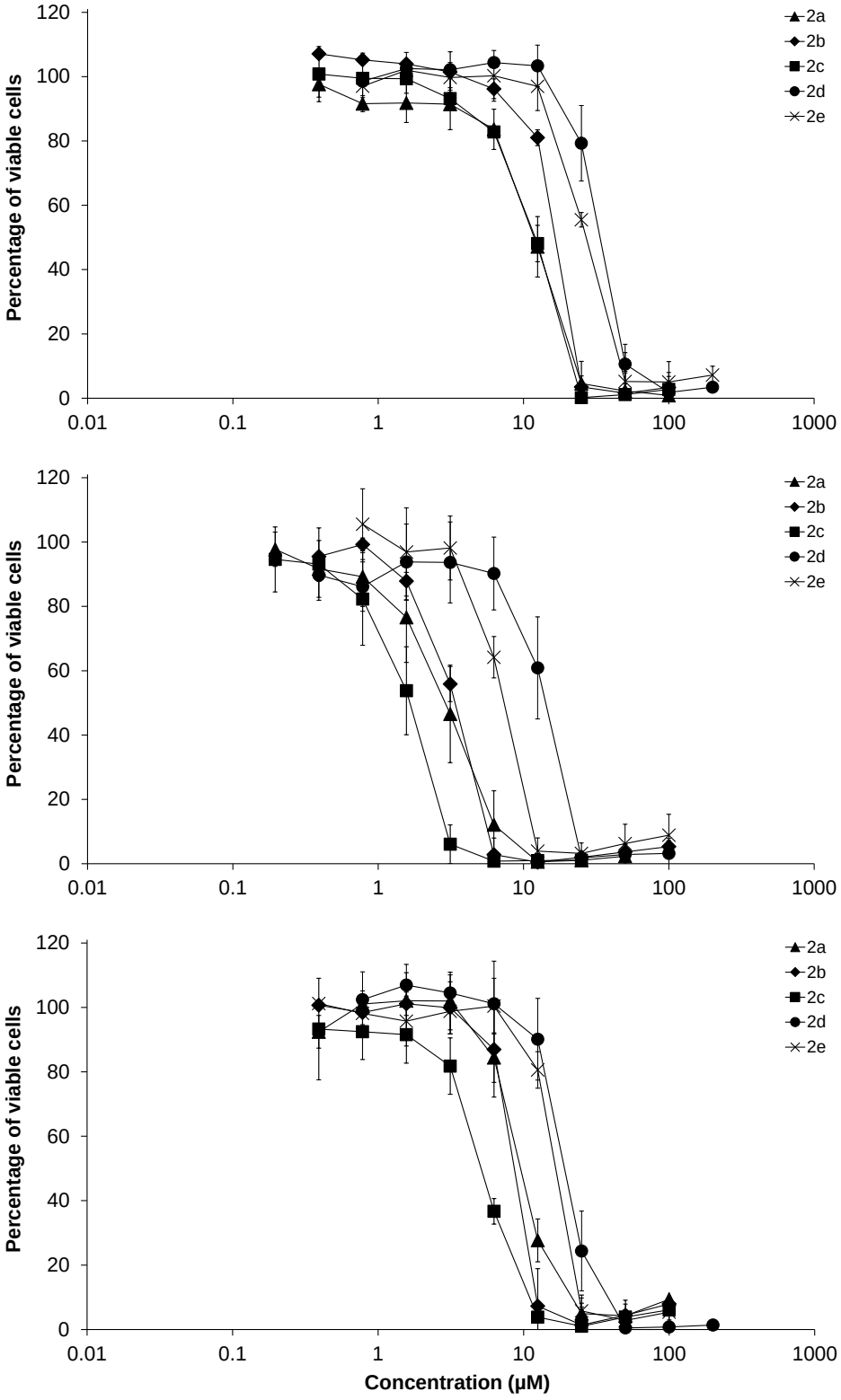

Figure S46: Concentration-effect curves of ruthenium complexes **2a**–**2e** in A549 (top), CH1/PA-1 (center) and SW480 cells (bottom) relative to untreated controls (100%). Values are means ± standard deviations from at least three independent MTT assays (exposure time: 96 h).

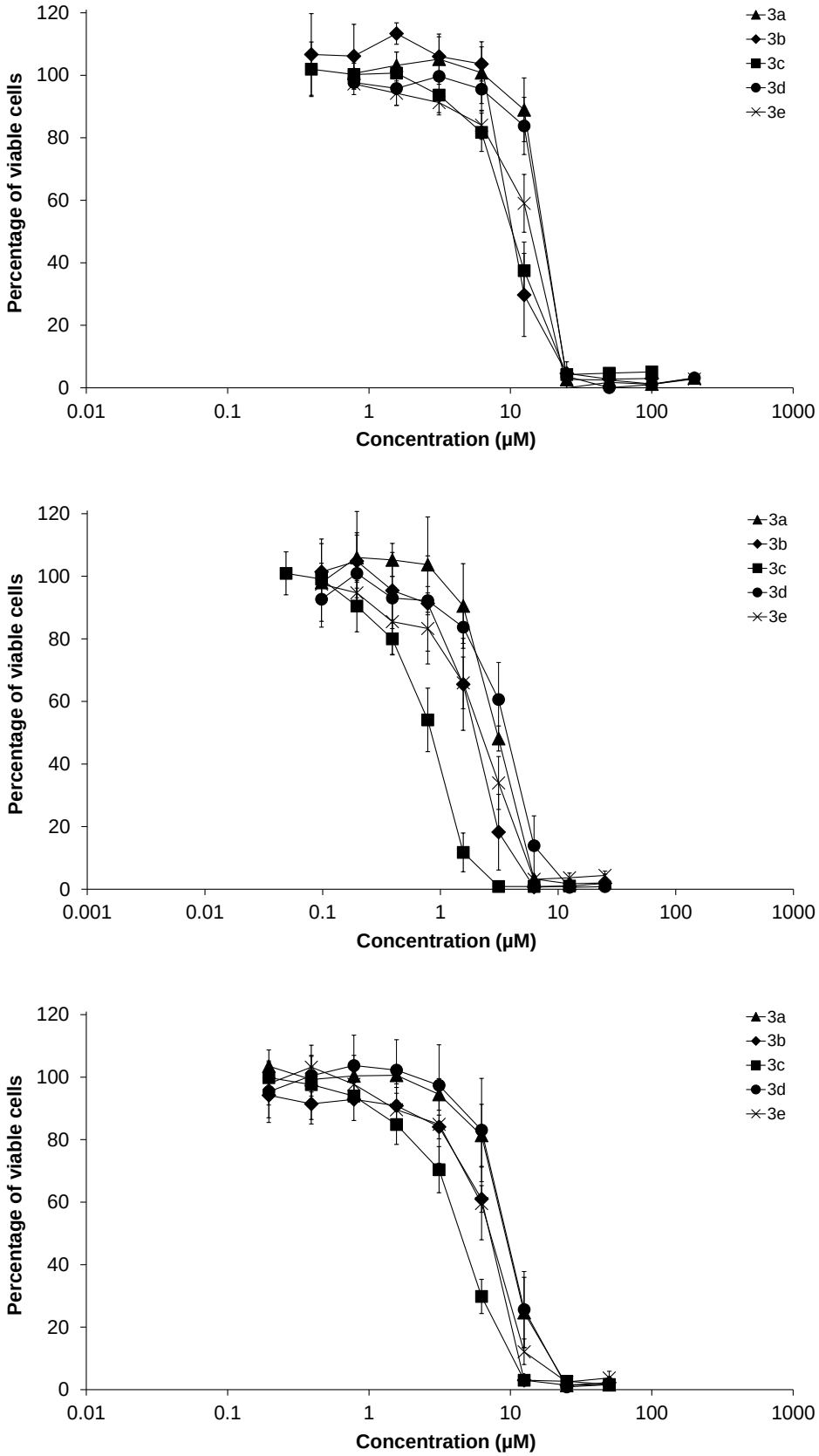

Figure S47: Concentration-effect curves of osmium complexes **3a**–**3e** in A549 (top), CH1/PA-1 (center) and SW480 cells (bottom) relative to untreated controls (100%). Values are means ± standard deviations from at least three independent MTT assays (exposure time: 96 h).

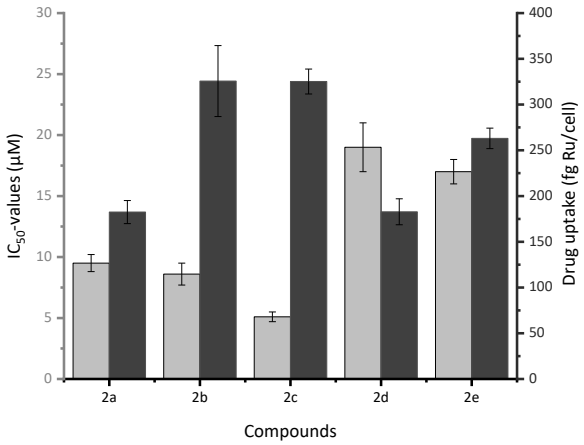

Figure S48: Dependency of cytotoxicity (IC_{50} values, light grey) on cellular accumulation (Ru/cell, dark grey) of ruthenacycles **2a–e**.

7. G-quadruplex interaction studies

Table S9: Oligonucleotide sequences. In dsDNA, Heg linker is [(-CH_2-CH_2-O-)$_6$].

Name	Sequence
c-*KIT*1 (FRET)	5'-/56-FAM/AGG GAG GGC GCT GGG AGG AGG G/36 TAMSp/3'
c-*MYC* (FRET)	5'-/56-FAM/TGG GGA GGG TGG GGA GGG TGG GCA AGG/36 TAMSp/3'
dsDNA (FRET)	5'-/56-FAM/ TAT AGC TA-Heg-TATA GCT ATA /36 TAMSp/3'
c-*KIT*1	5'-AGG GAG GGC GCT GGG AGG AGG G-3'
c-*MYC*	5'-TGA GGG TGG GTA GGG TGG GTA A-3'

Table S10: $\Delta T_{1/2}$ values of 0.2 µM c-*KIT1,* c-*MYC*, dsDNA upon interaction with metal complexes at 1.0, 2.0, 4.0 and 6.0 µM concentration. The results represent the average of three separate experiments, each conducted in duplicate. Concentration of DNA is reported in strand. Uncertainty is ≤0.5 for the $\Delta T_{1/2}$ reported. $\Delta T_{1/2} < \pm 0.5$ are reported as 0. n.a. = not available.

c-*KIT1*				
	1.0 µM	**2.0 µM**	**4.0 µM**	**6.0 µM**
2a	-0.6	-0.6	1.2	12.7
2c	-0.7	-1.4	-1.4	0
2d	-1.3	-2.2	1.7	9.0
c-*MYC*				
	1.0 µM	**2.0 µM**	**4.0 µM**	**6.0 µM**
2a	0.9	2.5	8.4	14.3
2c	3.5	8.6	15.0	18.0
2d	1.1	1.9	6.1	11.2
dsDNA				
	1.0 µM	2.0 µM	4.0 µM	6.0 µM
2a	n.a.	n.a.	0	n.a.
2c	n.a.	n.a.	0	n.a.
2d	n.a.	n.a.	0	n.a.

Table S11: Docking free energies of binding with c-*KIT1* G4.

	Kcal/mol (1st pose)	Kcal/mol (2nd pose)	Kcal/mol (3rd pose)
2a (*R*)	-7.48	-7.06	-7.01
2a (*S*)	-6.37	-5.92	-5.90
2c (*R*)	-8.61		
2c (*S*)	-7.84	-7.80	-7.53
2d (*R*)	-7.97	-7.20	-6.57
2d (*S*)	-6.73	-6.45	-6.20

Table S12: Docking free energies of binding with c-*MYC* G4.

	Kcal/mol (1st pose)	Kcal/mol (2nd pose)	Kcal/mol (3rd pose)
2a (*R*)	-7.77	-7.65	
2a (*S*)	-7.55	-6.72	-6.41
2c (*R*)	-9.04	-8.66	
2c (*S*)	-8.72	-8.20	
2d (*R*)	-7.97	-7.69	
2d (*S*)	-8.01	-7.10	-6.81

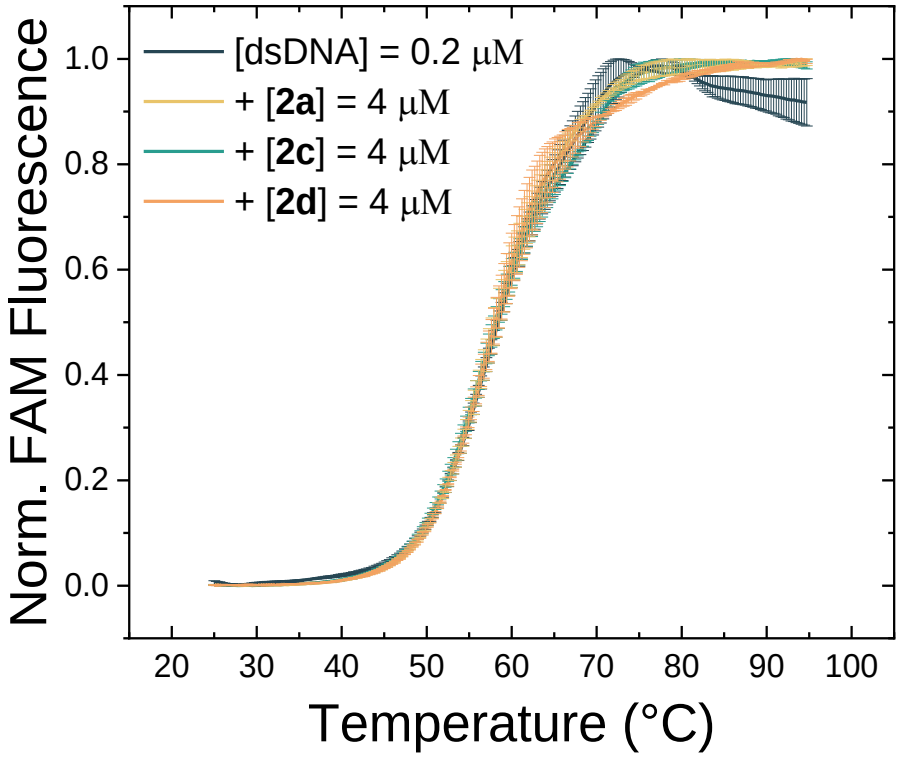

Figure S49: FRET melting profiles of dsDNA oligonucleotide (0.2 μM) upon interaction with the indicated compounds at the indicated concentration.

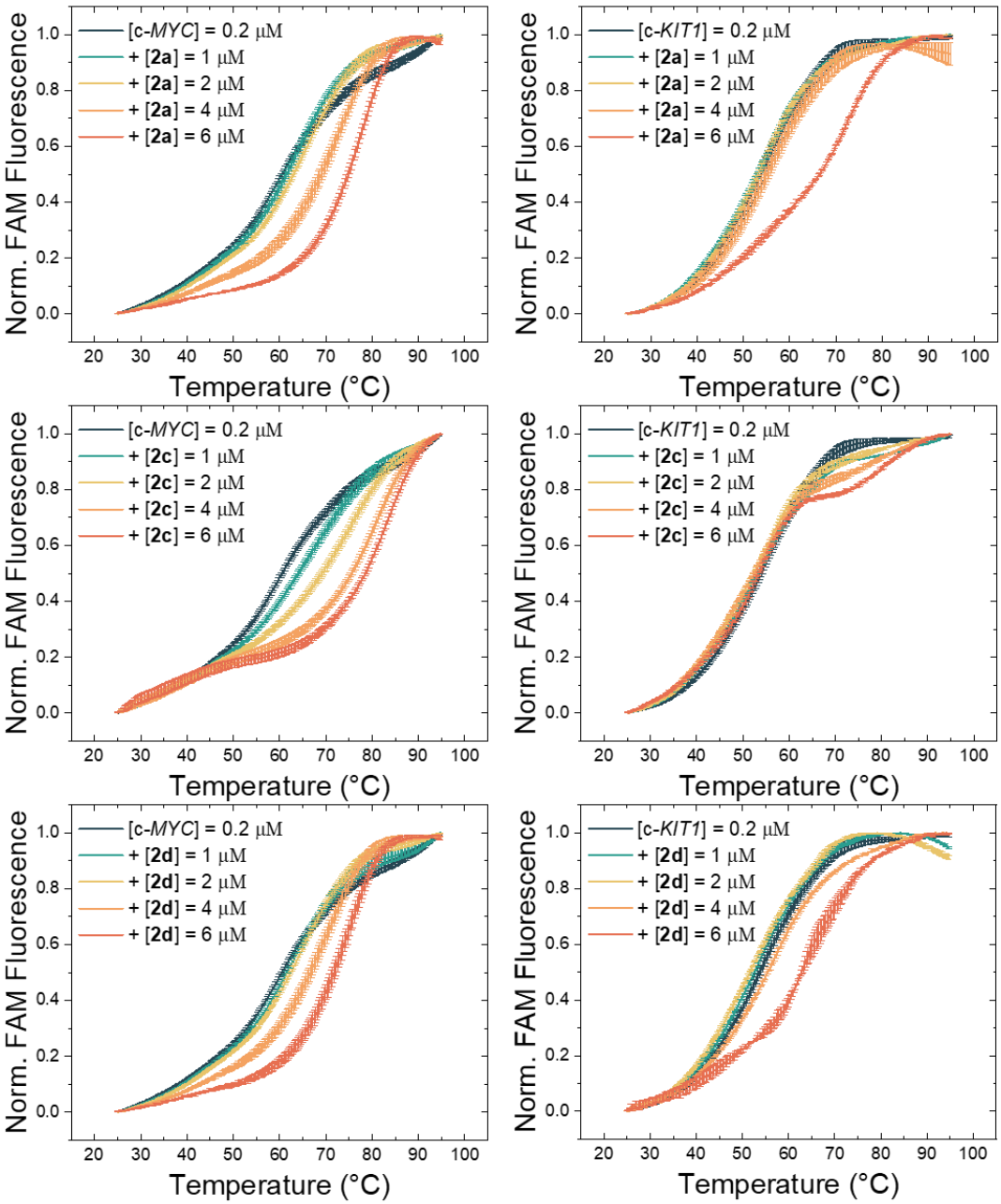

Figure S50: FRET melting profiles of *c-MYC* and *c-KIT1* G4s (0.2 µM) upon interaction with the indicated compounds at the indicated concentration values.

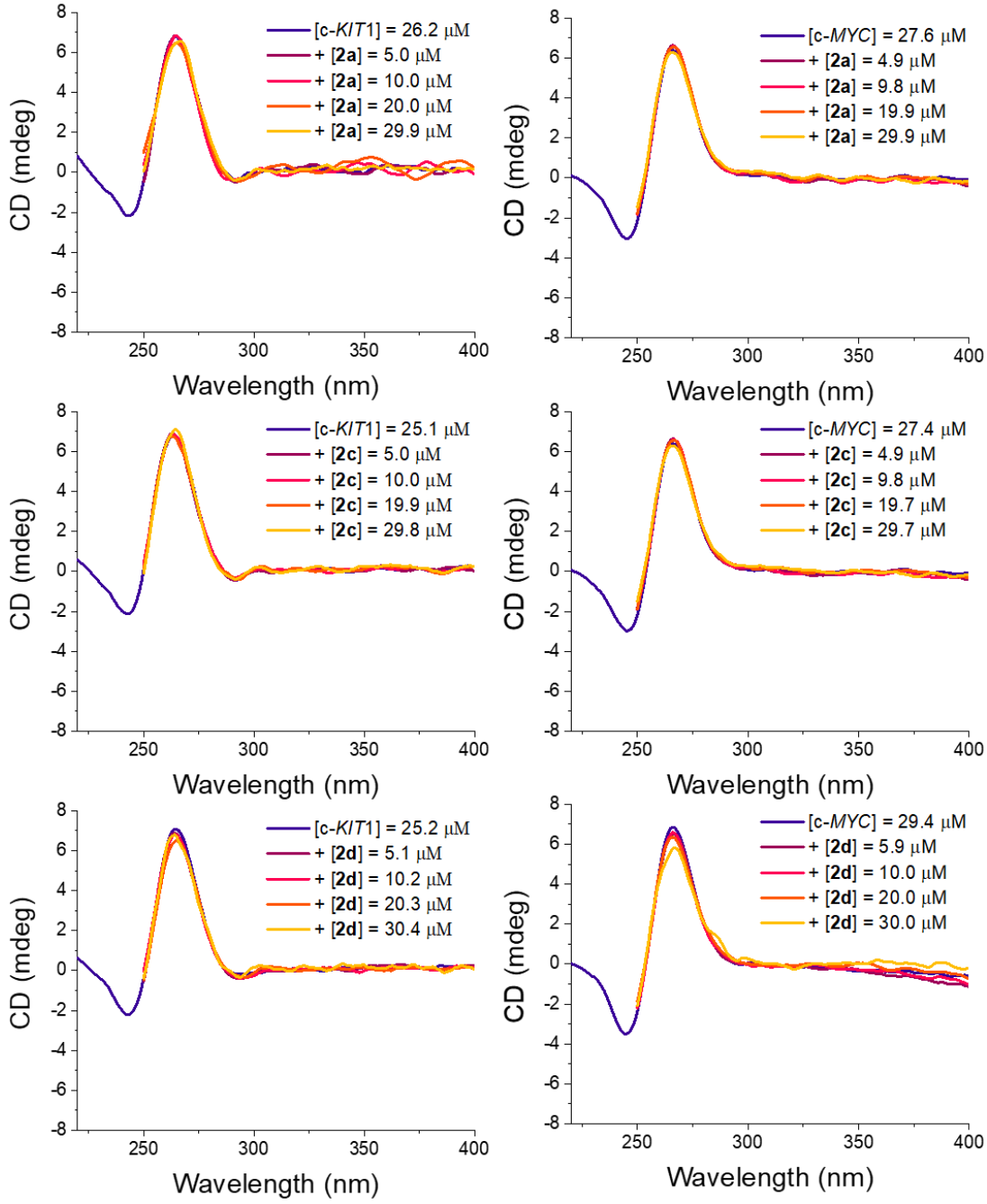

Figure S51: CD spectra of *c-KIT1* (left column) and *c-MYC* (right column) in the presence of increasing aliquots of **2a**, **2c** and **2d** at the indicated concentrations. Concentration of the oligonucleotides is reported in bases. When the metal-based compounds are in solution, the cut-off of the spectra was set at 250 nm due to the presence of DMF as co-solvent (% < 1.7%).

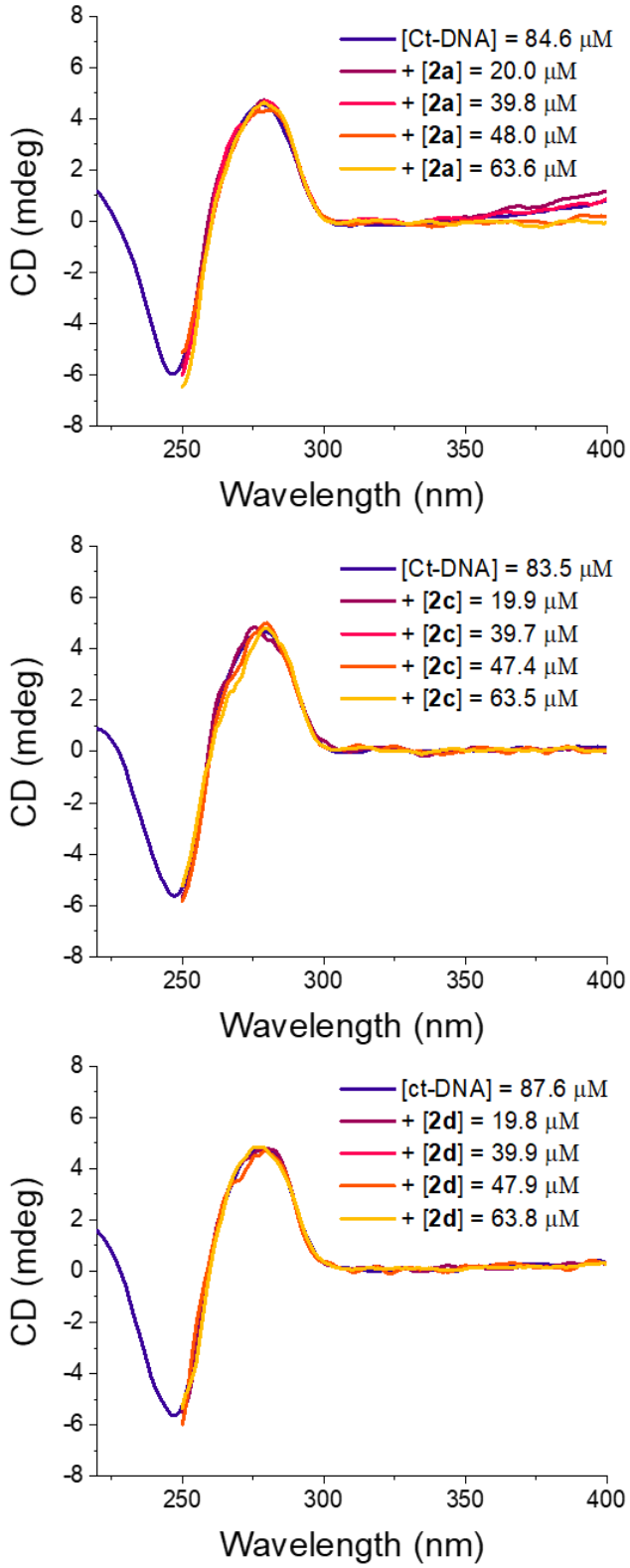

Figure S52: CD spectra of ct-DNA in the presence of increasing aliquots of **2a**, **2c** and **2d** at the indicated concentrations. Concentration of ct-DNA is reported in bases. When the metal-based compounds are in solution, the cut-off of the spectra was set at 250 nm due to the presence of DMF as co-solvent (% < 1.7%).

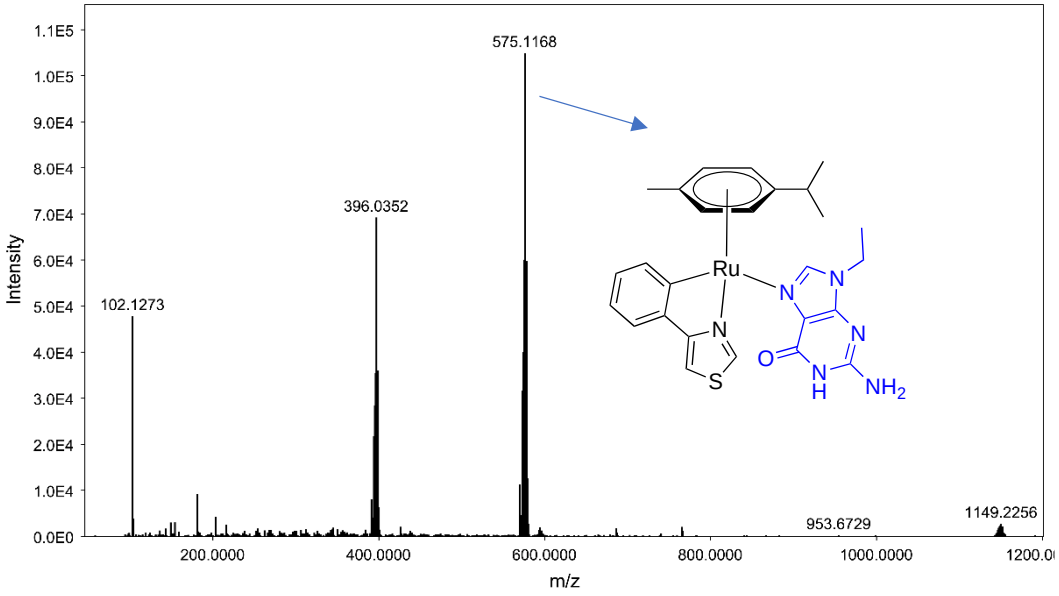

Figure S53: Mass spectrum of 9-ethylguanine incubated with **2a**. Final concentrations in MeOH/H_2O before injection were 0.2 mM for the metal compound and 0.6 mM for 9-EtG. Mass of 9-EtG-**2a** adduct: found 575.1168, calced.: 575.1167.

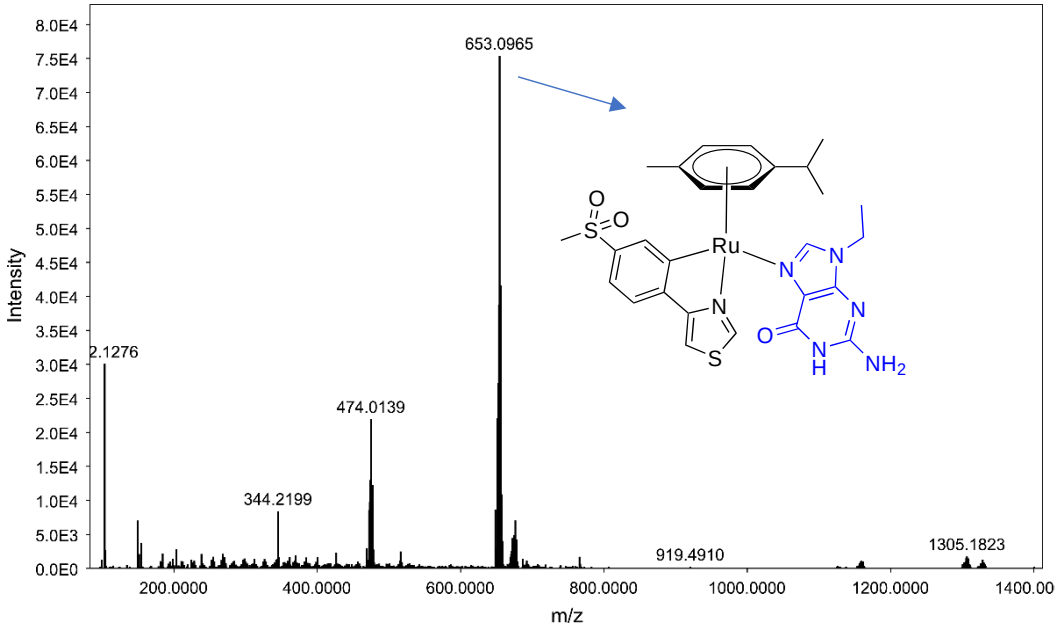

Figure S54: Mass spectrum of 9-ethylguanine incubated with **2c**. Final concentrations in MeOH/H_2O before injection were 0.2 mM for the metal compound and 0.6 mM for 9-EtG. Mass of 9-EtG-**2c** adduct: found 653.0995, calced.: 653.0943.

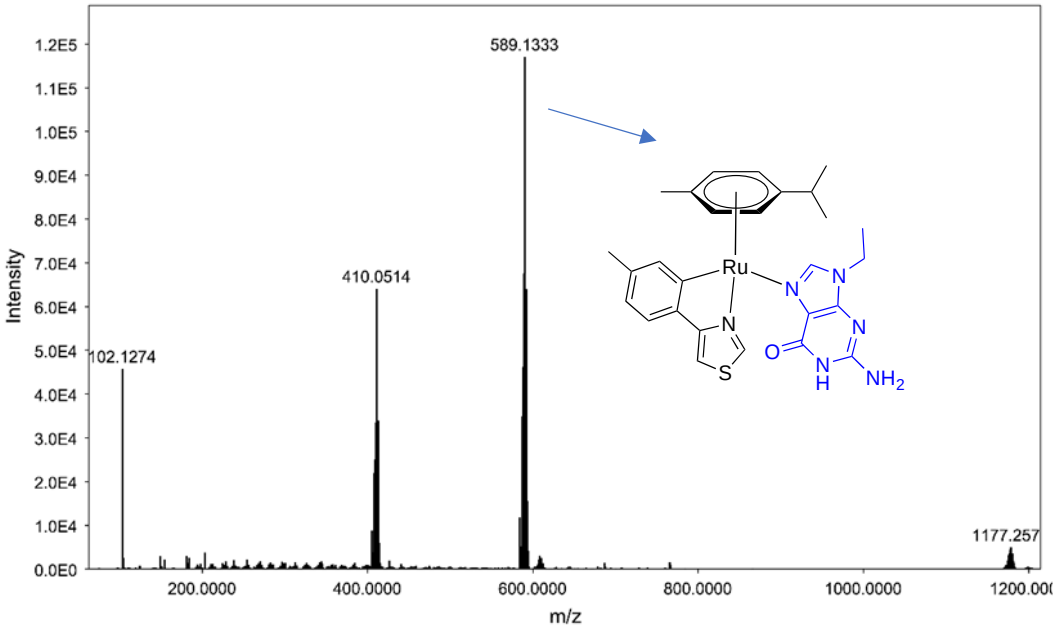

Figure S55: Mass spectrum of 9-ethylguanine incubated with **2d**. Final concentrations in MeOH/H_2O before injection were 0.2 mM for the metal compound and 0.6 mM for 9-EtG. Mass of 9-EtG-**2d** adduct: found 589.1333, calced.: 589.1324.

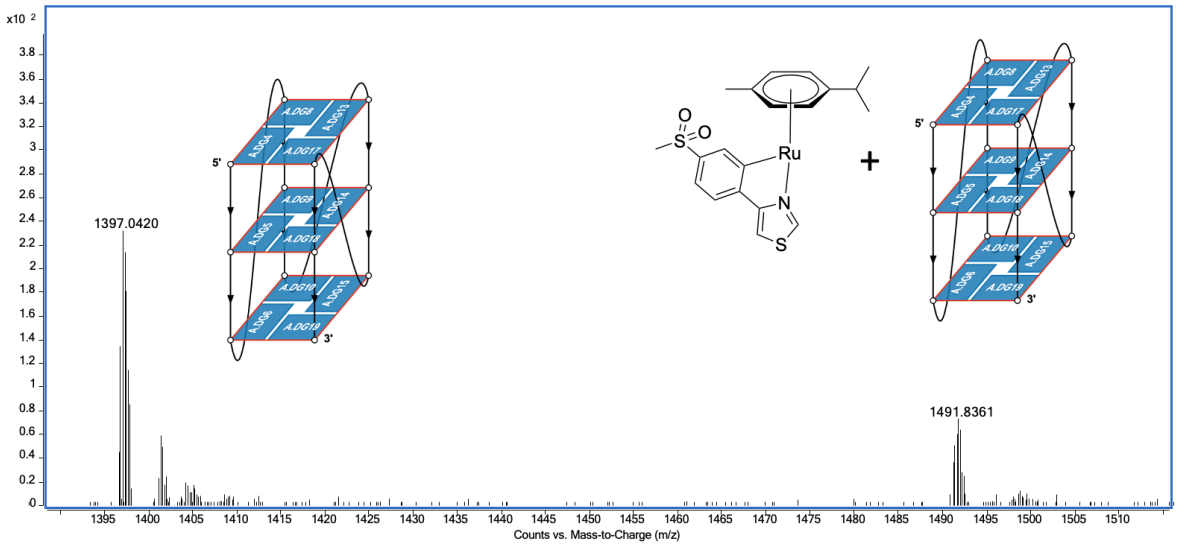

Figure S56: Mass Spectrum of **2c** incubated with c-*MYC* for 2 h at room temperature. Five charged mass of c-MYC: found: 1397.2403, calced: 1397.2318 (M-H^- for $C_{220}H_{270}O_{131}N_{95}P_{21}$.) Five charged mass of **2c**-c-*MYC* adduct: found: 1491.8361, calced: 1491.8332 (M-H^- for $C_{220}H_{270}\ O_{131}\ N_{95}P_{21}C_{20}H_{21}NO_2RuS_2$).

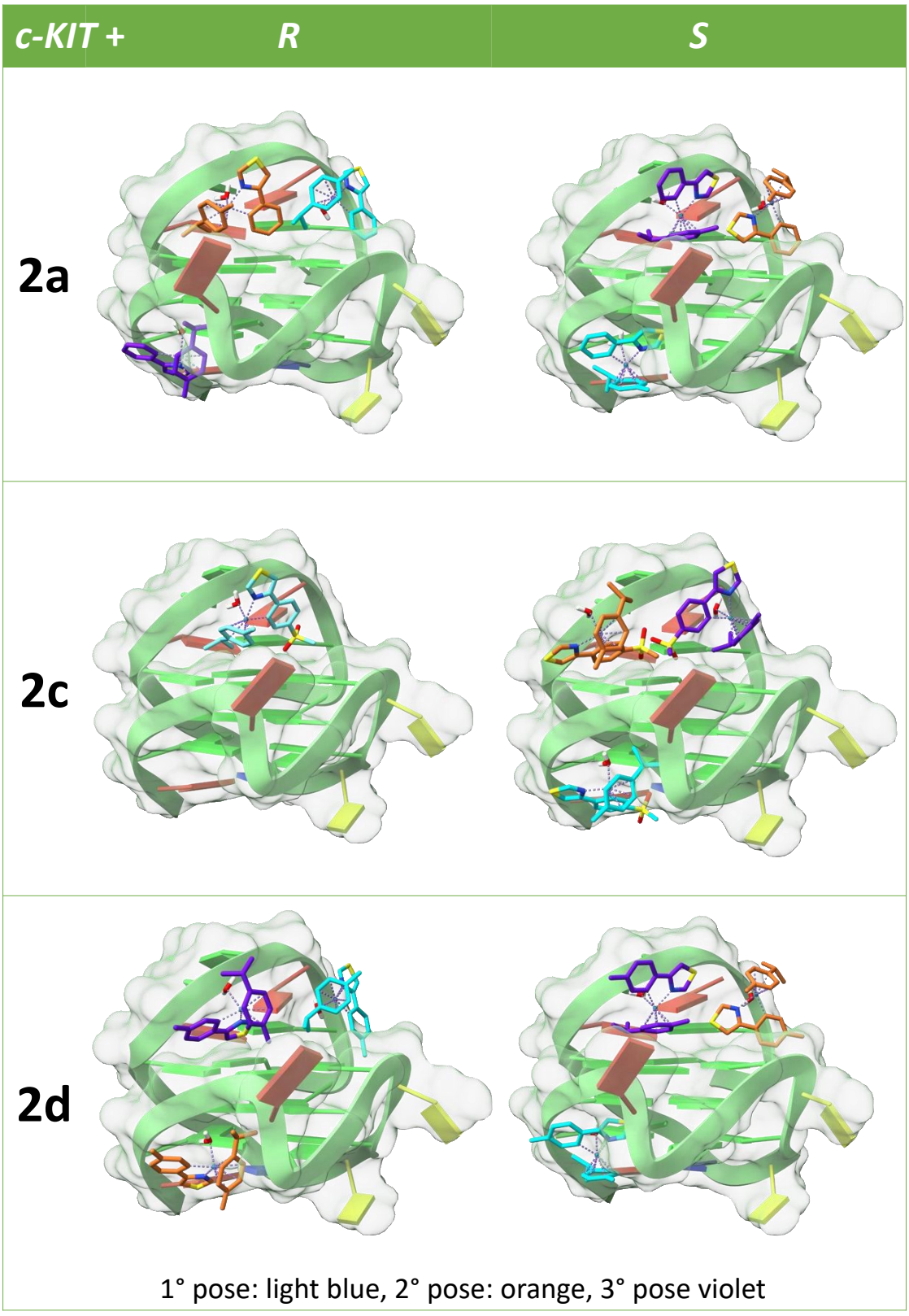

Figure S57: Cartoons showing possible binding sites of both enantiomers of **2a**, **2c** and **2d** with c-*KIT1* G4 (PDB id: 2O3M).

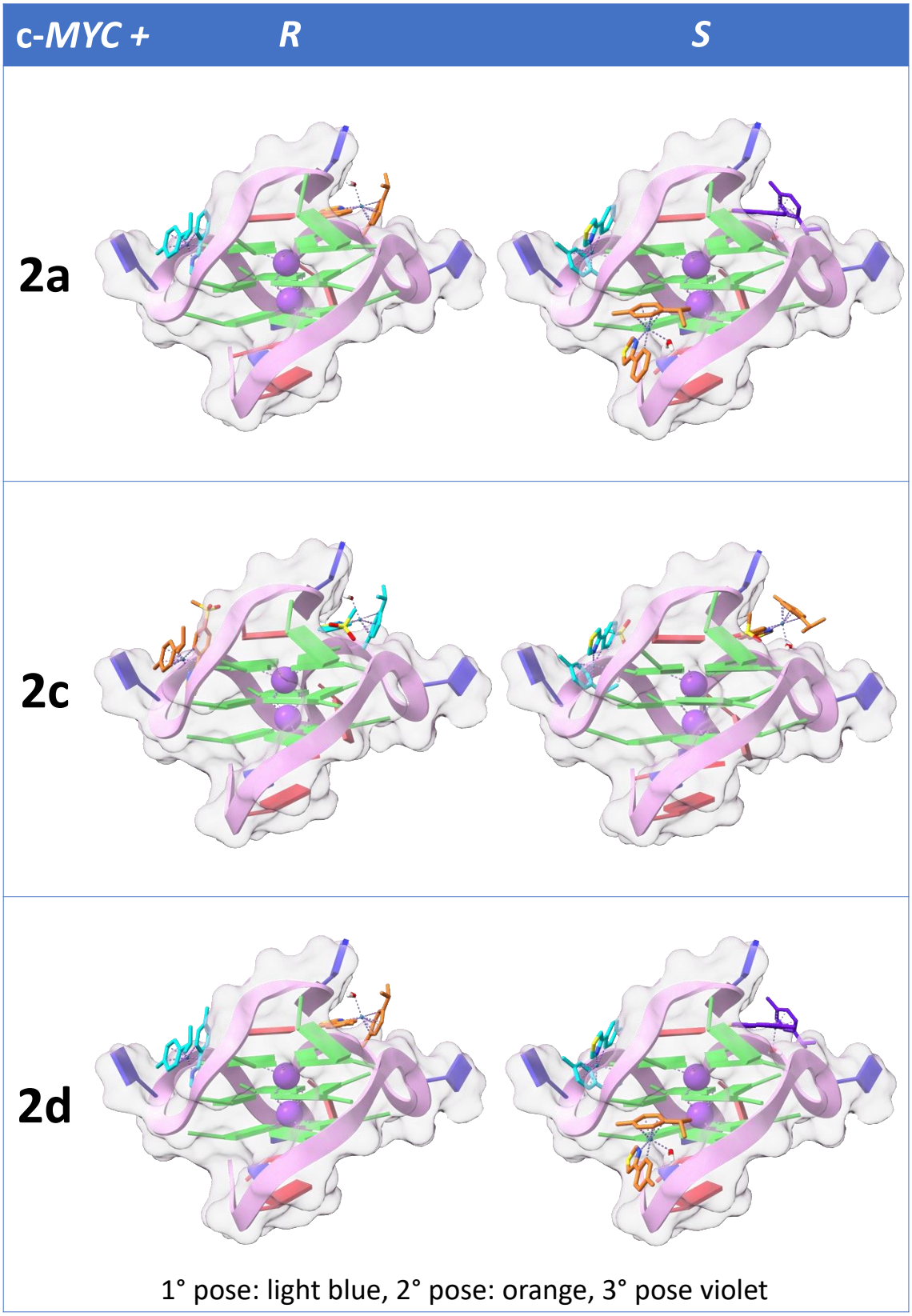

Figure S58: Cartoons showing possible binding sites of both enantiomers of **2a**, **2c** and **2d** with c-*MYC* G4 (PDB id: 1XAV).

8. Amino acid interaction study

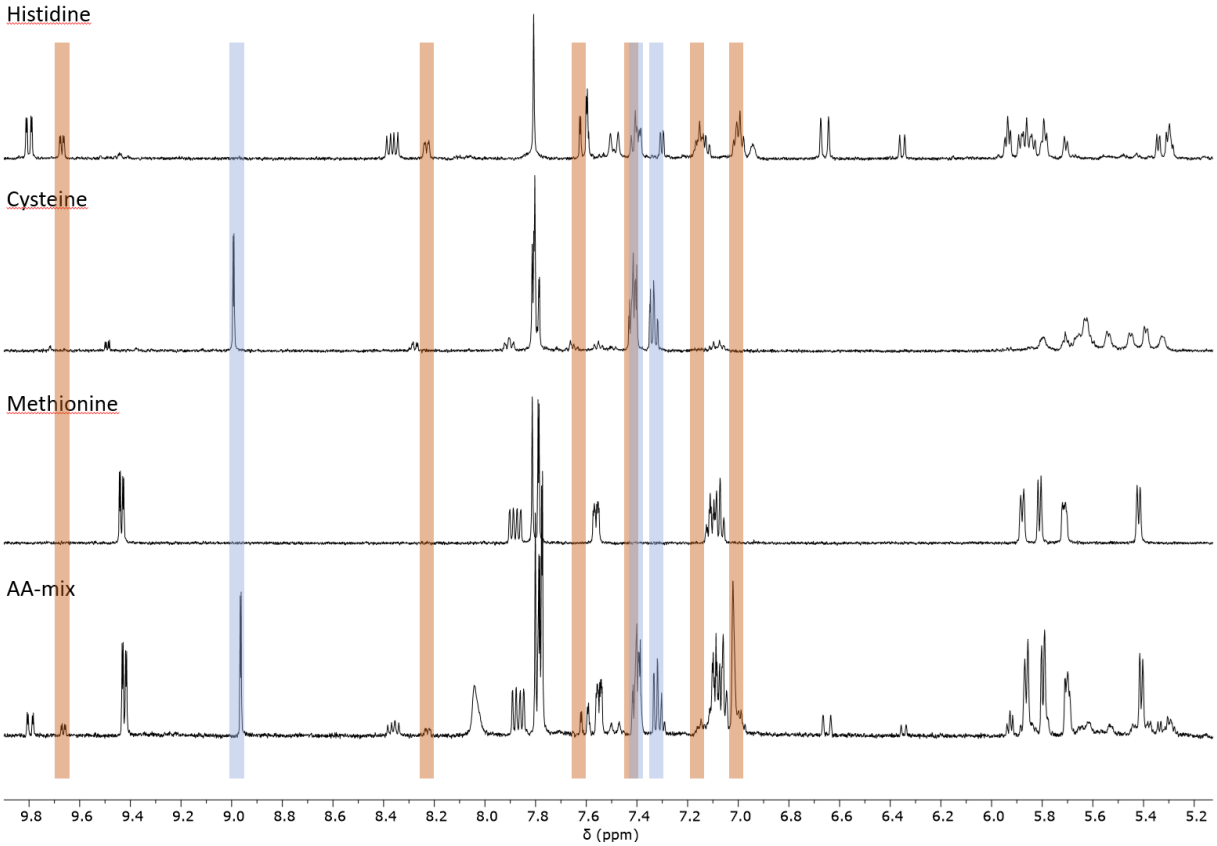

Figure S59: ^{1}H-NMR (10% d_7-DMF in D_2O, aromatic region) of **2a** incubated with protected amino acids histidine (first row), cysteine (second row), methionine (third row) and a 1:1:1 mixture of the mentioned amino acids for 24 h (red bar = protons of unconverted **2a**, blue bar = protons of free ligand **1a**).

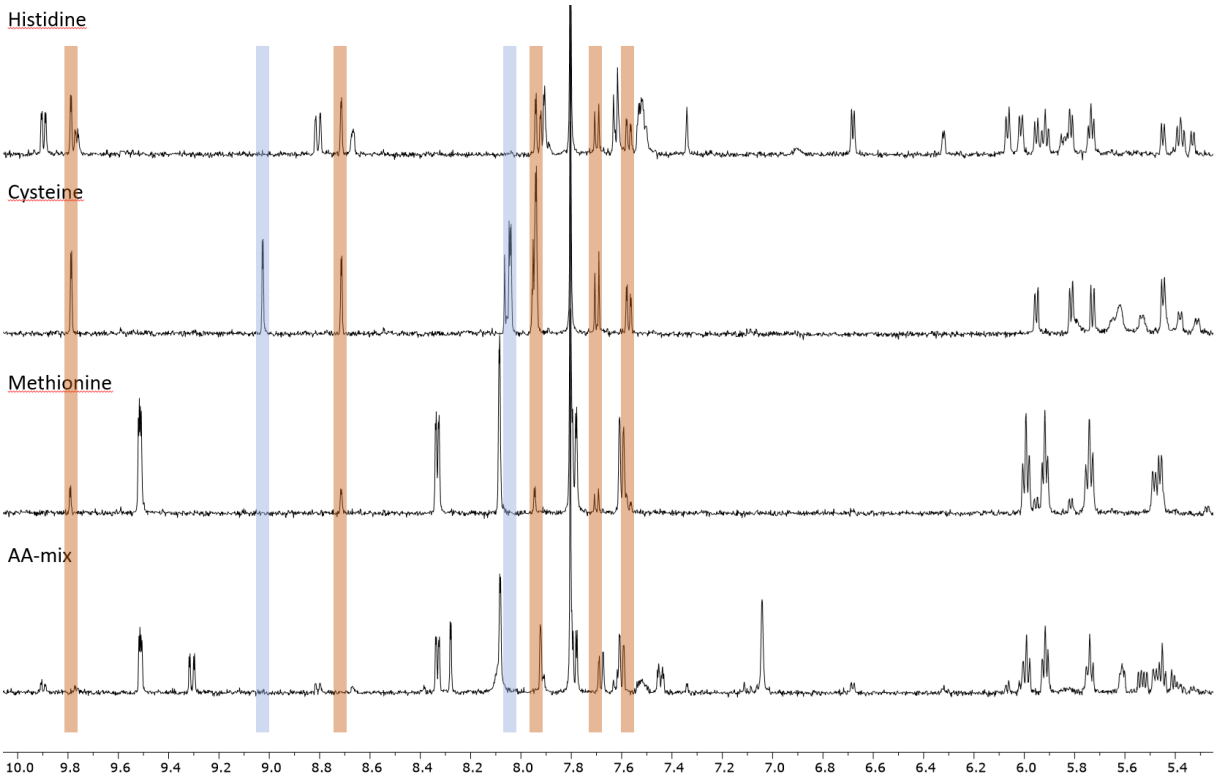

Figure S60: ^{1}H-NMR (10% d_7-DMF in D_2O, aromatic region) of **2c** incubated with protected amino acids histidine (first row), cysteine (second row), methionine (third row) and a 1:1:1 mixture of the mentioned amino acids for 24 h (red bar = protons of unconverted **2c**, blue bar = protons of free ligand **1c**).

9. Cell cycle investigation

Table S13: Cell cycle analyses results (exposure time: 24 h). Cell cycle phase distribution: G1/G0, S and G2/M relative count frequency (in %). The results are means ± standard deviations.

	Negative control	2c			2d			3c			3d		
Conc., µM	0	10	20	40	5	10	20	2.5	5	10	2.5	5	10
G1/G0, %	56 ± 3	58 ± 3	46 ± 9	45 ± 10	56 ± 5	54 ± 2	51 ± 5	51 ± 3	40 ± 8	55 ± 5	46 ± 3	53 ± 6	47 ± 2
S, %	32 ± 3	33 ± 3	28 ± 1	30 ± 7	35 ± 6	28 ± 4	29 ± 3	33 ± 3	45 ± 11	33 ± 2	38 ± 5	35 ± 5	32 ± 2
G2/M, %	16 ± 2	13 ± 1	36 ± 9	21 ± 2	12 ± 1	19 ± 2	24 ± 5	21 ± 3	20 ± 7	17 ± 6	19 ± 4	14 ± 3	23 ± 3

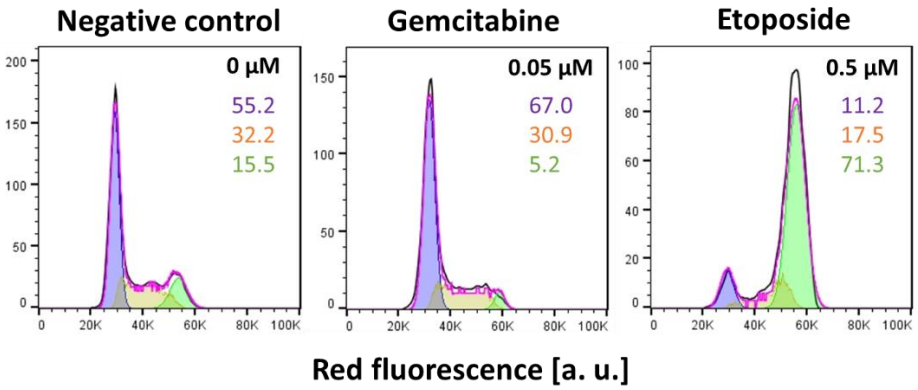

Figure S61: The effect of gemcitabine and etoposide on cell cycle frequency distribution. The frequency (Y-axis, counts) is plotted versus red fluorescence intensity of PI-stained SW480 cell nuclei upon 24 h exposure. At given concentrations gemcitabine is inducing the G1/G0 phase inhibition, while etoposide is arresting the cell cycle in G2/M phase.

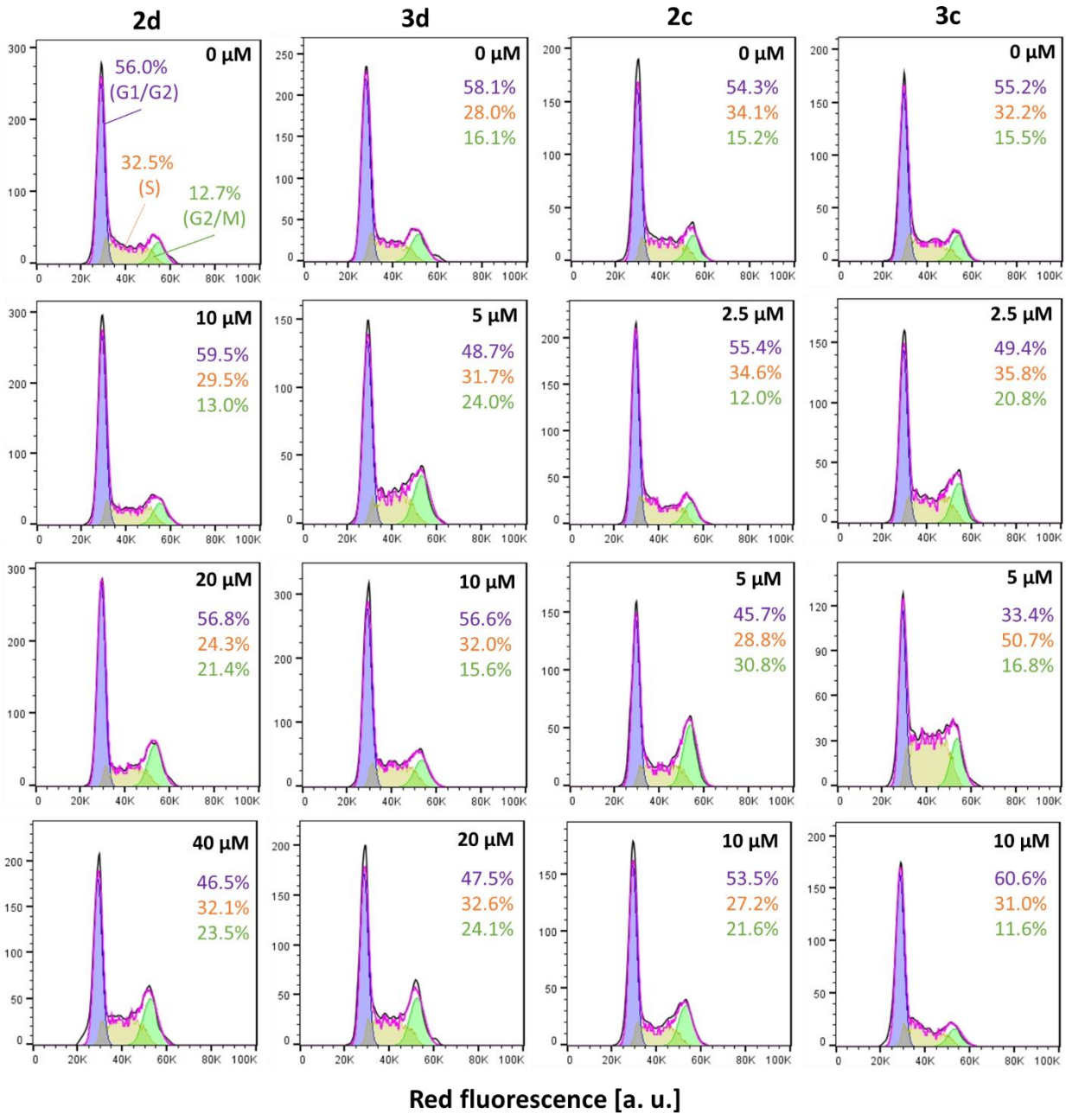

Figure S62: Cell cycle frequency distribution histograms (one experiment). The frequency (Y-axis, counts) is plotted versus red fluorescence intensity of PI-stained SW480 cell nuclei upon 24 h incubation with test compounds (**2c,d**, **3c,d**). The stacked values represent the corresponding cell cycle phase distribution in % (G1/G0 – violet, S – orange-yellow, G2/M – green).

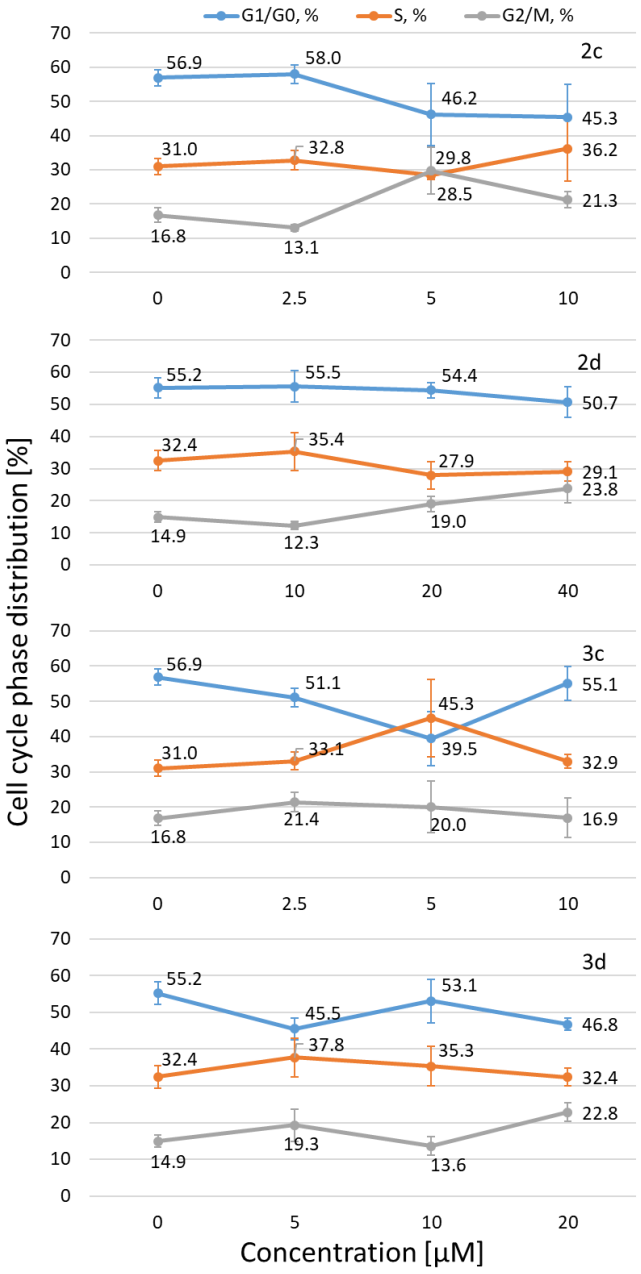

Figure S63: The effect of the compounds (**2c,d**, **3c,d**) on SW480 cell cycle phase distribution upon 24 h treatment. The data-points are means of three independent experiments and error bars represent the corresponding standard deviations.

10. Apoptosis

Table S14: Induction of apoptosis and necrosis of compounds **2c,d** and **3c,d** in SW480 cells after 24 h and 48 h at different concentrations (0.5 x IC_{50}, 1 x IC_{50}, 2 x IC_{50} and 10 x IC_{50}).

			24h incubation			48h incubation		
compound	concentration		average	stdv	Σ	average	stdv	Σ
untreated control		necrotic cells [%]	1.16	0.35		0.76	0.28	
		late apoptotic cells [%]	1.39	0.16	2.80	0.86	0.35	1.83
		early apoptotic cells [%]	1.40	0.45		0.97	0.39	
		viable cells [%]	96.07	0.58		97.25	0.35	
positive control	0.5 µM	necrotic cells [%]	6.32	1.66		2.38	1.20	
		late apoptotic cells [%]	89.60	1.47	90.04	96.70	1.82	97.05
		early apoptotic cells [%]	0.44	0.29		0.35	0.12	
		viable cells [%]	3.63	1.63		0.58	0.52	
2c	2.5 µM	necrotic cells [%]	1.10	0.41		0.99	0.41	
		late apoptotic cells [%]	1.31	0.40	3.05	1.55	0.84	3.28
		early apoptotic cells [%]	1.75	0.31		1.73	0.17	
		viable cells [%]	95.87	0.81		95.73	1.33	
	5 µM	necrotic cells [%]	0.97	0.03		0.83	0.30	
		late apoptotic cells [%]	1.50	0.47	3.33	1.45	0.47	3.70
		early apoptotic cells [%]	1.83	0.26		2.25	0.46	
		viable cells [%]	95.70	0.36		95.43	0.64	
	10 µM	necrotic cells [%]	0.90	0.25		0.87	0.22	
		late apoptotic cells [%]	1.23	0.55	4.10	2.25	0.65	9.65
		early apoptotic cells [%]	2.87	0.53		7.41	3.03	
		viable cells [%]	95.00	1.11		89.43	3.44	
	50 µM	necrotic cells [%]	2.85	1.02		4.63	1.90	
		late apoptotic cells [%]	8.80	2.26	10.31	19.07	5.75	21.41
		early apoptotic cells [%]	1.51	0.07		2.34	1.02	
		viable cells [%]	86.83	3.33		73.97	7.79	
2d	10 µM	necrotic cells [%]	0.92	0.15		0.85	0.42	
		late apoptotic cells [%]	1.57	0.98	2.84	1.39	0.13	2.70
		early apoptotic cells [%]	1.27	0.01		1.31	0.25	
		viable cells [%]	96.25	1.06		96.45	0.78	
	20 µM	necrotic cells [%]	0.88	0.31		0.72	0.27	
		late apoptotic cells [%]	1.18	0.43	2.63	1.76	1.25	3.49
		early apoptotic cells [%]	1.45	0.57		1.73	0.49	
		viable cells [%]	96.50	0.70		95.77	1.96	
	40 µM	necrotic cells [%]	0.89	0.37		0.61	0.15	
		late apoptotic cells [%]	1.97	0.54	3.97	1.91	0.59	5.44
		early apoptotic cells [%]	2.01	1.13		3.53	2.27	
		viable cells [%]	95.13	1.91		93.97	2.91	
	200 µM	necrotic cells [%]	6.06	3.14		2.10	1.23	

		late apoptotic cells [%]	89.47	6.18	89.80	95.93	2.64	96.91
		early apoptotic cells [%]	0.33	0.16		0.97	0.87	
		viable cells [%]	4.13	3.07		1.01	0.60	
3c	2.5 µM	necrotic cells [%]	0.80	0.34	3.17	0.66	0.10	3.53
		late apoptotic cells [%]	1.36	0.75		1.04	0.14	
		early apoptotic cells [%]	1.81	0.59		2.49	0.64	
		viable cells [%]	96.03	1.29		95.80	0.53	
	5 µM	necrotic cells [%]	0.58	0.20	2.67	0.51	0.09	4.35
		late apoptotic cells [%]	0.94	0.43		1.00	0.14	
		early apoptotic cells [%]	1.73	0.51		3.35	0.52	
		viable cells [%]	96.77	0.90		95.17	0.32	
	10 µM	necrotic cells [%]	0.60	0.15	3.64	1.32	0.19	14.43
		late apoptotic cells [%]	1.34	0.23		4.13	0.49	
		early apoptotic cells [%]	2.30	1.92		10.30	3.04	
		viable cells [%]	95.77	1.96		84.23	2.71	
	50 µM	necrotic cells [%]	4.13	2.87	11.06	6.83	3.32	19.66
		late apoptotic cells [%]	8.16	5.14		16.13	4.59	
		early apoptotic cells [%]	2.90	2.89		3.52	1.88	
		viable cells [%]	84.80	6.24		73.50	6.27	
3d	5 µM	necrotic cells [%]	0.77	0.21	3.17	0.56	0.07	3.26
		late apoptotic cells [%]	1.30	0.58		0.96	0.17	
		early apoptotic cells [%]	1.87	0.31		2.30	0.26	
		viable cells [%]	96.07	0.85		96.17	0.12	
	10 µM	necrotic cells [%]	0.86	0.28	3.37	0.46	0.04	4.69
		late apoptotic cells [%]	1.45	0.60		1.22	0.20	
		early apoptotic cells [%]	1.91	0.92		3.47	1.43	
		viable cells [%]	95.77	1.65		94.87	1.50	
	20 µM	necrotic cells [%]	1.16	0.31	9.54	1.65	0.45	24.73
		late apoptotic cells [%]	3.15	1.13		10.52	4.84	
		early apoptotic cells [%]	6.40	2.74		14.21	6.27	
		viable cells [%]	89.30	4.07		73.70	10.61	
	100 µM	necrotic cells [%]	7.43	1.08	91.88	4.90	1.17	92.82
		late apoptotic cells [%]	91.53	0.83		88.63	7.48	
		early apoptotic cells [%]	0.34	0.31		4.19	4.91	
		viable cells [%]	0.70	0.11		2.26	1.40	

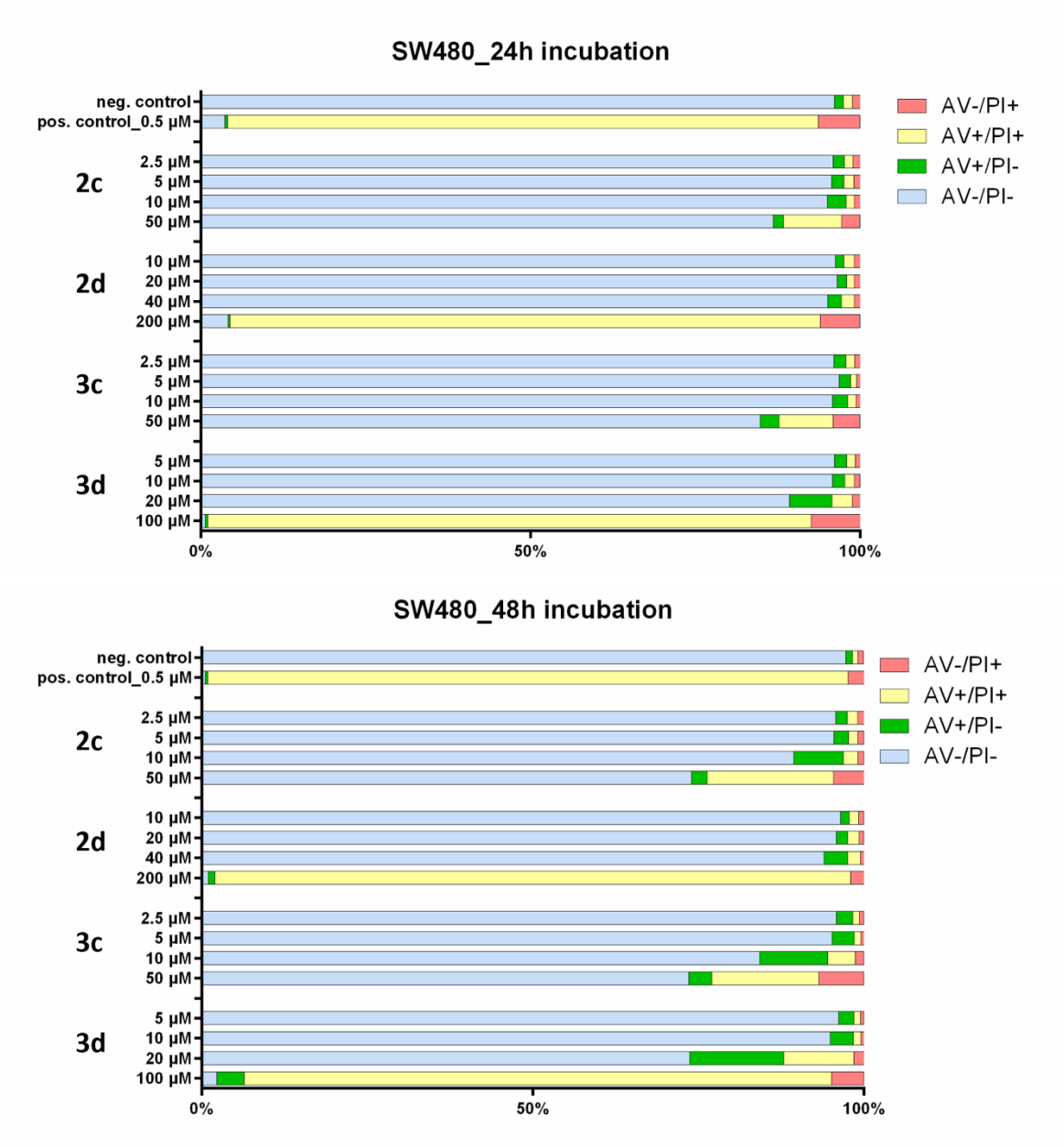

Figure S64: Apoptotic/Necrotic behavior of metalacycles **2c,d** and **3c,d** in SW480 cells after incubation for 24 h (top) and 48 h (bottom).